Time dependent Evolution of Massive Disks in Generalized Gravitational Potentials

Diplomarbeit

Institut für Theoretische Physik und Astrophysik
der Christian Albrechts Universität zu Kiel

February 2009

Meiert Willem Grootes

supervisor: Prof. Dr. W. J. Duschl

Time Dependent Evolution of Massive Disks in Generalized Gravitational Potentials

Massive accretion disks surrounding super massive black holes in the center of galaxies are assumed to be the source of the extremely high luminosities observed from these active galactic nuclei (AGN). The unified model for AGN, which explains a plethora of different cosmological objects, e.g. Seyfert I & II type galaxies, QSOs, and Blazars, bases on the concept of these massive disks. However, their development in the more generalized gravitational background potential created by their host galaxies remains unstudied. Additionally, the edges of the disks in these objects reside in the weak field regime of gravity, making them possibly susceptible to modifications in this regime.
I present results from simulations using a simple model of the time dependent evolution of these massive disks, showing that the embedding of these objects in background potentials, created by the distributions of mass in which they reside, has an effect on the evolution time of the system, as well as on the angular velocity and surface density profiles at the edge of the disk. I show that differences arise between systems using a cuspy dark matter halo and those using a dark matter halo with a constant density core and finally, that the development of systems, in which Modified Newtonian Dynamics (MOND) has been used as proxy for an acceleration scale based modification to Newtonian gravity, in the weak field limit is discernibly different from that of systems using a cold dark matter (CDM) model.

"There is a theory which states that if ever anybody discovers exactly what the Universe is for and why it is here, it will instantly disappear and be replaced by something even more bizarre and inexplicable. There is another theory which states that this has already happend".

Douglas Adams

Contents

1 Introduction

Gravity is the major driving force for evolution of any kind on large scales in the universe. The reciprocal attraction of mass leads to the decoupling of ever smaller regions from the expansion of the universe and hence to the formation of structure to ever larger degrees and lager relative overdensities.
However, if matter starts to collapse gravitationally towards a central point of some sort, it is highly likely that most, if not all, of this matter will carry some angular momentum with respect to the center of attraction. Even if this may not be the case in the earliest stages of the universe, after some evolution it certainly will be. However, according to Noether's theorem, angular momentum is always conserved, just like e.g. momentum and energy. Accordingly, matter can not gravitationally collapse with impunity, but rather is hindered by the conservation of its angular momentum, i.e. it cannot move further towards the center of gravity than a certain radius without shedding angular momentum in some way. Since, however, angular momentum is defined by the perpendicular distance to the axis of rotation, the collapse can continue in the direction parallel to this axis, thus forming disk-like structures of matter rotating about the object they are being attracted to.
The only way for the matter in these disks to continue its gravitationally driven infall onto the central object is to transfer angular momentum to material farther away from the center, enabling the remaining matter to move inward. This process is called accretion and the disk systems accretion disks.
Because of the fundamental nature of this process such systems are ubiquitous in the universe and appear on all scales. A multitude of astrophysical phenomena can be explained by this mechanism. Moving from small scales to ever larger ones, these phenomena include, e.g. Saturns rings, cataclysmic variables and planet & star formation, Seyfert galaxies, and Quasi Stellar Objects (QSOs). Although the fundamental processes are the same, these systems obviously differ in e.g scale, mass of the central object, and mass of the accretion disk. Whilst in the case of star formation one sees the gravitational collapse of a cold molecular cloud with a protostar forming, surrounded by an accretion disk, as shown in fig.(1), a model for the explanation of nova type cataclysmic variables starts with a close binary system in which one component is a white dwarf or a stellar mass black hole and the other component is a star which has grown beyond its Roché lobe. The matter from this star is then free to fall onto the companion, however, it forms an accretion disk due to its angular momentum. The matter thus slowly accretes onto the compact companion until it ignites a thermonuclear explosion, fig.(2). One of the most interesting fields of application for the accretion model is, however, that of Active Galactic Nuclei (AGN).
The standard model for an AGN is a super massive black hole (SMBH) at the center of a galaxy surrounded by an accretion disk. This disk is the result of large amounts of gas being forced into the center of the galaxy, e.g by a merger event between two galaxies. The accretion mechanism allows a substantial fraction of the potential energy of the gas to be transformed into radiation, resulting in luminosities, which easily surpass those of entire galaxies, ranking AGN amongst the most luminous objects in the observed universe. This idea allows phenomena such as Seyfert I & II galaxies, QSOs, Quasars, and Blazars

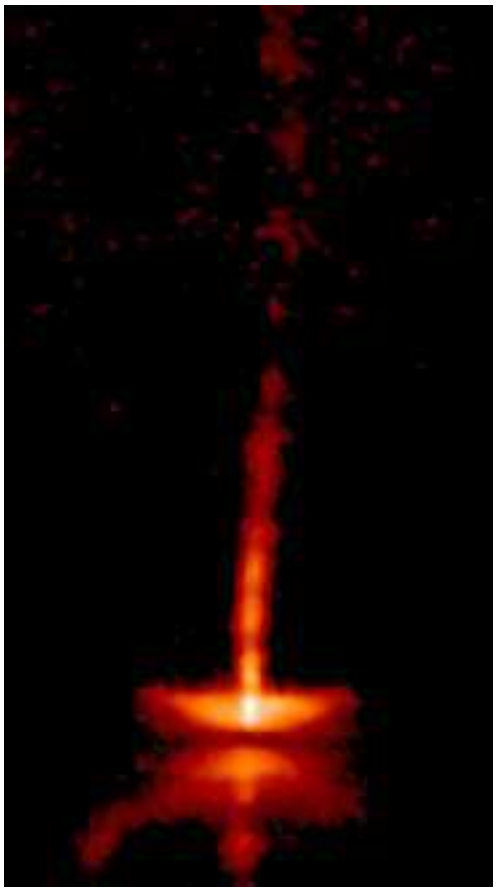

Figure 1: *The Herbig-Haro object HH 30 in the Taurus-Auriga molecular cloud approximately 450 lightyears from Earth. The image shows dust above and below an optically thick disk being illuminated by the protostar at the center, as well as two jets emerging perpendicularly from the disk. The disk can be seen as a dark bar in the image. Credit: NASA, STScI, ESA*

to be explained by one model, where the type of the object depends on the inclination under which it is observed, the central mass, and the mass of the disk, and the size of the suurounding dust torus, and may be able to explain the observed anti-hierarchical growth of SMBH, whose observed peak in number-density lies at higher red-shift the more massive they are (Hasinger et al., 2005; Ueda et al., 2003).
Usually, however, the model does not include the astrophysical environment, i.e. host galaxy, in which the AGN is located, fig.(3). Furthermore, being systems which are dominated by gravitational forces, but usually not considered in this context, they are also prime candidates for use in testing different gravitational models/potentials, and might help shed light on the discussion of the dark matter problem.

Figure 2: *Artists impression of a nova type cataclysmic variable. The red giant star has extended beyond its Roché lobe and material is being accreted onto the white dwarf companion, where it accumulates and ignites in a thermonuclear explosion. Credit D. A. Hardy & STFC*

1.1 Aim

This work presents a computational model and uses it to calculate the time dependent evolution of circumnuclear accretion disks in generalized gravitational potentials. These include embedding potentials such as those generated by host galaxies, as well as those generated by the dark matter halos in which the standard model embeds the luminous galaxies. On the other hand, modifications to the Newtonian theory of gravity are studied. The aim is to discern, whether the time dependent evolution of accretion disks around SMBHs differs based upon the scenario used. The code includes a prescription for viscosity in the disk - the β-viscosity prescription (Duschl et al., 2000) - as well as a treatment of self-gravity in the monopole approximation.
Using this model, the evolution timescales as well as the general evolution of quantities such as the surface density, radial velocity, and angular velocity are calculated and compared for different scenarios.

Figure 3: *Superimposed radio and optical image of the host galaxy of the nearest AGN Centaurus A. The AGN is located at the center of the galaxy which is seen nearly edge on. Credit VLA, Hubble*

2 Theory of Accretion Disks

Accretion disks have been found or are expected in a variety of astrophysical scenarios. Although these ubiquitous systems may differ in size, mass, and type of accreting object, the basic processes governing their evolution are the same. This enables the creation of a basic, simplified model, that gives a reasonable representation of the system and includes the major processes. The differences observed in real accreting systems can be explained as modifications of the basic model, due to processes of greater complexity that, while important, only modify the result

2.1 Geometry of the problem

An accreting system basically consists of two major components, the central accreting object, e.g. a black hole, a white dwarf or some other massive object, and a disk of material being accreted. This material is usually assumed to be gaseous. Accordingly the systems consist of a more or less thin disk differentially rotating around a central object, with the axis of rotation being defined by the angular momentum initially carried by the accreting material and the direction of rotation of the central object. Ignoring other perturbing effects, the problem at hand, i.e the modeling of the disk, demonstrates aspects of cylindrical symmetry as is apparent in fig(4). Therefore, it is sensible to adopt a system of cylindrical coordinates, with the origin being located in the center of the accreting object and the z-axis being aligned with the main axis of rotation. For a given point in space $\vec{\mathbf{r}}$ one obtains:

$$\vec{\mathbf{r}} \;=\; \vec{\mathbf{r}}(s, \phi, z) \tag{1}$$

with s being the radial coordinate in the plane perpendicular to the axis of rotation, ϕ being the azimuthal coordinate and z being the position along the axis of rotation. Using this system together with the model assumptions presented below allows a simplification of the equations governing the system.

2.2 Self - Gravity

As stated in sec.(2.1), an accreting system consists of a central object and a disk of material being accreted, however, depending upon what kind of system is being studied, the relation of the masses of these components can vary. In a system where the greatest part of the total mass is located in the central object and only a small fraction is contained in the disk, the entire gravitational potential and hence the gravitational acceleration/force will be dominated by the central object, with the contribution made by the disk being negligible. This case is called a non-self-gravitating(NSG) disk, and the system displays Keplerian rotation. On the other hand, in a system, in which the mass of the disk is very much larger than that of the central object, the gravitational force will contain a sizeable contribution resulting from the disk itself. If the gravitational force is dominated by the disk itself, one speaks of a fully self-gravitating(FSG) disk.
In between both of these cases are a wide variety of accreting systems in which self-gravity

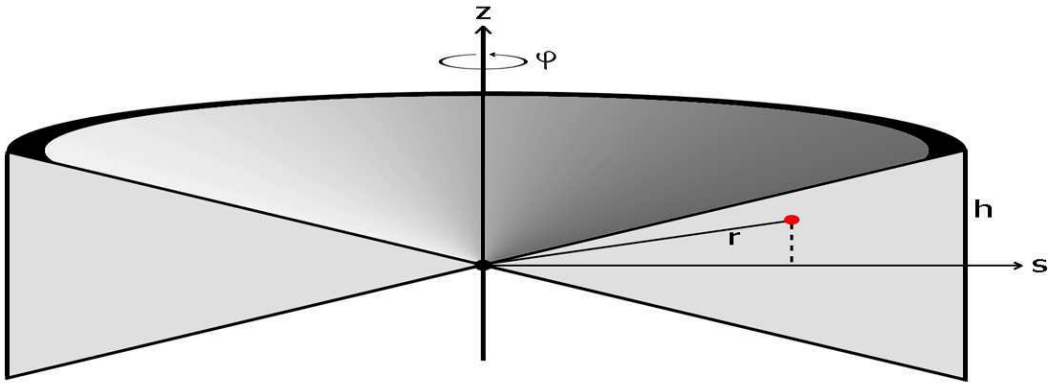

Figure 4: *Schematic depiction of an accretion disk around a central black hole. The disk is assumed to be rotationally symmetrical and display symmetry with respect to the s,ϕ -plane. For the model a thin disk has been assumed, so $h_{\max}(s) \ll s$. Cylindrical coordinates adapted to the symmetry are used to describe the system. Credit: I. V. Hinz, taken from Hinz (2008)*

plays a more or less important role, especially since for example in the case of FSG systems it is very well possible that the innermost regions are nonetheless dominated by the central mass. This also implies, that a sort of transitory region exists. Therefore it is of great importance for massive systems, that some scheme to implement self-gravity be included. In the work at hand this has been done. The method employed is explained in sec.(2.4) and sec.(5.1).

2.3 Viscosity

The central mechanism, enabling the formation of accretion disks and the accretion of mass onto central objects, is the transfer of angular momentum outward, allowing material to be accreted. Since the accretion disk consists mainly of gaseous material, it is to be expected that it will rotate differentially in some form akin, even if not identical, to Keplerian rotation. The self-gravity of the disk leads to deviations from keplerian rotation. The differential rotation means that different areas of the disk rotate at different angular velocities, leading to friction in the disk. This friction, which is described by viscosity, exerts torque on the material, facilitating the transport of angular momentum. The viscous stress is given by the viscous stress tensor $\sigma_{\text{visc};ik}$ as:

$$\sigma_{\text{visc};ik} = \eta \left(\frac{\partial v_i}{\partial x_k} + \frac{\partial v_k}{\partial x_i} - \frac{2}{3} \frac{\partial v_j}{\partial x_j} \delta_{ik} \right) + \zeta \frac{\partial v_j}{\partial x_j} \delta_{ik} \tag{2}$$

with $i, j, k \in \{r, \phi, z\}$ denoting the components of the tensor in the chosen coordinate sys-

tem and the derivatives being of the correct form for that system (Landau & Lifschitz, 1959). The first term with the coefficient η denotes the stress due to shearing-viscosity and the second term with the coefficient ζ denotes the stress due to bulk-viscosity. The relevant viscosity due to differential rotation is the dynamical viscosity or shearing viscosity with the parameter η, or in an often employed, slightly reformulated form known as kinematic viscosity, with the parameter $\nu = \eta/\rho$, where ρ denotes the density. The bulk-viscosity is mainly of importance for shocks, and is therefore negligible for the problem at hand, as well as not being well-understood, hence the value of ζ has been set to zero.
However, although it is established that the kinematic viscosity is central to the evolution of accretion disks, especially those which are predominantly gaseous, the exact nature of the viscosity in these objects remains unknown. In order to achieve the accretion rates corresponding to the observed luminosities of e.g. Active Galactic Nuclei (AGN), a large amount of angular momentum must be transferred relatively quickly. The characteristic timescale on which this occurs is the viscous time scale $\tau_{\text{visc}} = s^2/\nu$. However, the molecular viscosities of known materials are orders of magnitude too small to facilitate the necessary transport of angular momentum on realistic timescales.
It is usually assumed that some kind of turbulent viscosity exists in the disks, that operates more efficiently than the molecular viscosity, allowing the observed phenomena to be explained. However, the underlying physics of this viscosity remain a subject of debate and investigation, although magnetic instabilities are often cited (Hawley et al., 1995; Fromang et al., 2004).
Given the lack of a conclusive first principle model for turbulent viscosity, it is acceptable to choose a parametrization of turbulent viscosity based on sensible assumptions. The first such approach suggested and in wide spread use is the α-viscosity prescription (Shakura & Syunyaev, 1973). However, this prescription leads to problems for self-gravitating disks (Duschl et al., 2000; Paczynski, 1978).
An alternative to the α-viscosity has been proposed by Duschl et al. (2000). Starting from the historical results of instabilities in Couette-Taylor flows between co-axial rotating fluids, in which turbulence is generated at high Reynolds numbers $\mathfrak{R} = sv_\phi/\nu$ due to a purely hydrodynamic instability, and based on the reanalysis of these results (Richard & Zahn, 1999) in terms of a turbulent viscosity, they arrive at a viscosity prescription of the form:

$$\nu = \beta s v_\phi \tag{3}$$

Furthermore, as Lynden-Bell & Pringle (1974) and Thompson et al. (1977) have pointed out, the occurrence of turbulence will lead to an increase in viscosity, until the Reynolds number is reduced to a value $\mathfrak{R}_{\text{crit}}$, so that β is a constant satisfying

$$\beta \lesssim \frac{1}{\mathfrak{R}_{\text{crit}}} \sim 10^{-3} - 10^{-2} \tag{4}$$

where the numerical value for β is based upon laboratory values for $\Re_{crit}$. This β viscosity alleviates the problems mentioned and contains the α-viscosity in the non-self-gravitating disk limit (see Duschl et al., 2000).
Consequently β-viscosity has been used as the prescription for the turbulent kinematic viscosity.

2.4 Model Assumptions

In creating the model, used to investigate the time dependent evolution of accretion disks, some assumptions have been made with respect to the disk system. These assumptions, while simplifying the system, do not fundamentally alter the evolution and are justified for use in a preliminary investigation.
The main assumptions made are:

1. Azimuthal symmetry $\longrightarrow \quad \partial/\partial\phi \;=\; 0$
2. Symmetry with respect to the s-ϕ-plane
3. Geometrical thinness of the disk, i.e. $h \;=\; z_{max} \;<<\; s$
   This assumption will be modified to a razor thin disk later.
4. Monopole approximation for self gravity:
   The mass $M_d(s)$ of the disk inside the radius s is added to the central monopole for calculations outside of the radius s.

Furthermore, the only forces taken into account are the viscous forces in the disk and the gravitational forces working on the system.

2.5 Basic Equations

An accretion disk consists mainly of gaseous material and can be treated as a continuous fluid with macroscopically defined local physical properties such as e.g. density ρ and velocity $\vec{\mathbf{v}}$. The evolution of these properties is governed by the conservation equations with respect to (angular) momentum and mass, as well as equations describing possible external forces influencing the system, e.g gravitational forces.
The conservation equations are usually cast in the mathematical form of continuity equations.

2.5.1 Conservation of Mass

The equation describing the conservation of mass as a continuity equation is given by:

$$\frac{d}{dt}\rho \;=\; \frac{\partial}{\partial t}\rho + \nabla\cdot(\rho\vec{\mathbf{v}}) \;=\; 0 \tag{5}$$

Where ρ is the mass density and $\vec{\mathbf{v}}$ is the velocity vector. This equation states, that the change of the density in a unit volume is the sum of inflow and outflow of material through the surface of that unit volume - eq.(5) being the differential form of the equation.
Based on the assumptions made above concerning the dimensions of the disk as well as its symmetry, it is useful to switch to the vertically integrated form of eq.(5):

$$\int_{-\infty}^{\infty}\frac{d\rho}{dt}dz \;=\; \int_{-\infty}^{\infty}\frac{\partial\rho}{\partial t}dz + \int_{-\infty}^{\infty}\nabla\cdot(\rho\vec{\mathbf{v}})dz \;=\; 0 \tag{6}$$

Employing cylindrical coordinates and making use of the assumptions and the fact that, since all the integrals are absolutely convergent, the order of differentiation and integration may be reversed, one obtains:

$$\frac{d}{dt}\Sigma \;=\; \frac{\partial}{\partial t}\Sigma + \frac{1}{s}\frac{\partial}{\partial s}\left(v_s\Sigma s\right) + \frac{\partial}{\partial z}\underbrace{\int_{-\infty}^{\infty}\rho v_z dz}_{\substack{\to\ 0\\ (s,\phi)\text{-symmetry}}} + \underbrace{\frac{\partial}{\partial\phi}\int_{-\infty}^{\infty}\rho v_\phi dz}_{\substack{\to\ 0\\ \partial/\partial\phi = 0}} \;=\; 0 \tag{7}$$

Where $\Sigma = \int_{-\infty}^{\infty}\rho dz$ is the vertically integrated surface density and the v_i with $i \in \{s,\ \phi,\ z\ \}$ are the components of the velocity.
In its simplified vertically integrated form, as used for the model, eq.(5) consequently takes the following form:

$$\frac{d}{dt}\Sigma \;=\; 0 \;=\; \frac{\partial}{\partial t}\Sigma + \frac{1}{s}\frac{\partial}{\partial s}\left(v_s\Sigma s\right) \tag{8}$$

This equation links the evolution of the surface density of the disk with the radial motion of the gas, giving an “equation of motion” in radial direction.

2.5.2 Conservation of Angular Momentum

In addition to the conservation of mass, which is used to obtain the radial component of the equation of motion, the conservation of angular momentum is used to obtain the azimuthal component. In this work, the approach introduced by Shakura & Syunyaev (1973) and used by Pringle (1981) in their seminal papers has been adopted.
Using the model of a thin axisymmetric disk with a surface density $\Sigma(s,t)$, an azimuthal velocity $v_\phi = \omega s$ and a radial velocity v_s, consider an annulus at the radius s with a radial extent δs. The amount of angular momentum carried by the annulus is then given by:

$$L_{\text{an}} = 2\pi s \delta s \Sigma \omega s^2 \tag{9}$$

The angular momentum of the annulus can change over time by only two processes :

- The in- and outflow of material from the annulus carrying angular momentum
- The application of torque to the annulus

Thus one obtains an expression for the conservation of the angular momentum of an annulus:

$$\begin{aligned} \frac{\partial}{\partial t} L_{\text{an}} &= v_s(s,t) 2\pi s \Sigma(s,t) \omega(s,t) s^2 \\ &- v_s(s+\delta s,t) 2\pi (s+\delta s) \Sigma(s+\delta s,t) \omega(s+\delta s,t) (s+\delta s)^2 \\ &+ \mathfrak{G}(s,t) - \mathfrak{G}(s+\delta s,t) \end{aligned} \tag{10}$$

Where $\mathfrak{G}$ is the torque being exerted by an inner annulus on an outer one . Since the radial extent δs of the annulus is small in comparison to s, i.e. $\delta s \ll s$ equation (10) can be reformulated using a Taylor expansion to fist order in s as follows:

$$\frac{\partial}{\partial t}\left(s \delta s \Sigma(s,t) \omega(s,t) s^2\right) = -\frac{\partial}{\partial s}\left(v_s(s,t) s \Sigma(s,t) \omega(s,t) s^2\right) \delta s - \frac{1}{2\pi}\frac{\partial}{\partial s}\mathfrak{G}(s,t)\delta s \tag{11}$$

Division by δs then results in the azimuthal component of the equation of motion, however, the torque remains to be specified :

$$\frac{\partial}{\partial t}\left(s \Sigma \omega s^2\right) + \frac{\partial}{\partial s}\left(v_s s \Sigma \omega s^2\right) = -\frac{1}{2\pi}\frac{\partial}{\partial s}\mathfrak{G} \tag{12}$$

Therefore, it is now necessary to derive an expression for the torques exerted on each other by the annuli due to viscosity.
The stress tensor σ_{ik} is defined as follows and consists of the viscous stress tensor $\sigma_{\text{visc};ik}$ and the unit pressure tensor (Landau & Lifschitz, 1959):

$$\sigma_{ik} = -p\delta_{ik} + \sigma_{\text{visc};ik} \tag{13}$$

With δ_{ik} being the unit tensor and the viscous stress tensor taking the form presented in sec.(2.3) in eq.(2). The force acting on a surface can consequently be expressed as:

$$(F)_i = \sum_{k=1}^{3} \sigma_{ik} A_k = \sigma_{ik} A_k \tag{14}$$

Where $(F)_i$ are the components of the the force vector $\vec{\mathbf{F}}$ in the relevant coordinate directions and A_k are the components of the surface normal $\vec{\mathbf{A}}$ of the surface which the force is acting on, and Einstein's summation convention has been used in the last step.
To calculate the torques, the force being exerted tangentially to the annuli is of interest. With the model assumptions and using cylindrical coordinates the only non-negligible tangential components of the symmetrical tensor are $\sigma_{\phi s}$ and $\sigma_{s\phi}$, with $\sigma_{\phi s} = \sigma_{s\phi} = \eta s \frac{\partial \omega}{\partial s}$.
Thus the total torque exerted by an inner annulus on an outer one is given by:

$$\mathfrak{G} = -4\pi s^2 h \sigma_{\phi s} = -2\pi s^3 \Sigma \nu \frac{\partial \omega}{\partial s} \tag{15}$$

Where h is the half-thickness of the disk and $\nu = \eta/\rho$ is the kinematic viscosity coefficient. The viscous stress and, hence, the viscous torques are due to the annuli of gas "rubbing" against each other, due to their different angular velocities caused by the differential rotation. Accordingly, as has been pointed out (Hayashi & Matsuda, 2001), these quantities should vanish in the case of solid body rotation. Examination of eq.(15) shows that this is indeed the case.
Plugging eq.(15) back into eq.(12) one obtains the final form for the azimuthal equation of motion:

$$\frac{\partial}{\partial t}\left(s\Sigma\omega s^2\right) + \frac{\partial}{\partial s}\left(v_s s\Sigma\omega s^2\right) = \frac{\partial}{\partial s}\left(s^3\Sigma\nu\frac{\partial\omega}{\partial s}\right) \tag{16}$$

linking the evolution of the surface density with the radial and azimuthal velocities. Since the disk is assumed to be razor thin no equation for the vertical (z) component is necessary and this is the full set of equations of motion.

2.5.3 Poisson's Equation

The conservation of mass and angular momentum lead to the "equations of motion" for the system. However, in deriving these equations it has been implicitly assumed that the law of rotation $\omega(s,t)$ is known and that its derivatives can be calculated. In holding with the assumptions made, the only forces taken into account are the viscous forces and the gravitational force. The gravitational force is linked to the gravitational potential in such a manner, that the azimuthal velocity is given as:

$$\frac{v_\phi^2(s)}{s} = \omega(s)^2 s = -\frac{\partial \Phi}{\partial s} \tag{17}$$

and accordingly the law of rotation is given as:

$$\omega(s) = \sqrt{-\frac{1}{s}\frac{\partial \Phi}{\partial s}} \tag{18}$$

Where Φ is the gravitational potential. According to Poisson's equation the potential can be derived from the matter density distribution as follows:

$$\Delta\Phi - 4\pi G\rho \;=\; 0 \tag{19}$$

Where ρ is the mass density and G is the gravitational constant. Hence, knowledge of the density distribution allows the calculation of the potential and thus the gravitational force and rotation law at any point in the system. In the symmetry of the problem and using the assumptions made, eq.(19) simplifies to:

$$\frac{1}{s}\frac{\partial}{\partial s}\left(s\frac{\partial \Phi}{\partial s}\right) + \frac{\partial^2 \Phi}{\partial z^2} = 4\pi G\rho \tag{20}$$

2.6 Accretion Efficiency

Accretion disks, especially those in AGN, can be seen as "machines" converting potential energy into radiation. The potential energy of a mass m in the potential field created by a point mass M, with the potential being set to 0 at infinite distance from the mass M, is

given by:

$$E_{\mathrm{pot}}(r) = -\frac{GMm}{r} \tag{21}$$

Hence the difference in potential energy between two points r_1 and r_2 for a mass m is:

$$\Delta E_{\mathrm{pot}}(r_1, r_2) = \frac{GMm}{r_2} - \frac{GMm}{r_1} = (GMm)\,\frac{r_1 - r_2}{r_1 r_2} \tag{22}$$

If one assumes $r_1 \gg r_2$ or, to be more precise, assumes infall from $r_1 = \infty$, this simplifies to:

$$\Delta E_{\mathrm{pot}}(r_2) = \frac{GMm}{r_2} \tag{23}$$

This is the maximum amount of energy which can be transformed into radiation.
In an accretion scenario one can assume a more or less constant flow of material onto the accretor, represented as $\dot{M}$. Using this value one can obtain the maximum amount of energy that can be transformed into radiation per unit time by the accretion process, i.e. a luminosity $L_{\mathrm{acc,max}}$. If one considers a black hole as the accreting object, then r_2 can be roughly identified as the radius corresponding to the innermost stable circular orbit r_{isco} (this is derived for a test particle only), which is located at 3 Schwarzschild radii if one assumes the Schwarzschild metric, i.e. $r_{\mathrm{isco}} = 3r_{\mathrm{s}} = 6GM/c^2$. Using this expression one obtains:

$$L_{\mathrm{acc,max}} = \frac{\Delta E_{\mathrm{pot}}(r_s)}{\Delta t} = \frac{\dot{M}c^2}{6} \tag{24}$$

as the maximum conceivable accretion luminosity. However, during the infall not all energy can be transformed into radiation, since a large fraction is bound in the rotation of the disk material. Additionally, since the Schwarzschild radius does not define a solid surface, energy can be accreted beyond this radius, before it can be emitted, i.e escape from the disk. Therefore, the actual luminosity is smaller than the maximum luminosity. This can be described by adding a parameter to the maximum accretion luminosity. Subsuming leading multiplicative factors into the parametrization one obtains:

$$L_{\mathrm{acc}} = \widetilde{\eta} L_{\mathrm{acc,max}} = \eta \dot{M} c^2 \tag{25}$$

for the accretion luminosity. As is obvious from the expression, the accretion process is capable of transforming a sizeable fraction of the rest mass energy into radiation. Following the argumentation presented in Frank, King, & Raine (2002), a reasonable estimate for the efficiency appears to be $\eta \approx 0.1$. As a comparison the efficiency obtained by nuclear burning in stars is on the order of $\eta = 0.007$.

2.7 A razor-thin Disk Model

Combining the results derived previously, one arrives at a set of equations, which are capable of describing the time dependent evolution of the model consisting of a razor-thin disk around a massive central point-like, object with gravity taken into account in the form of a monopole approximation. The equations of the system present a set of coupled differential equations for the properties Σ, v_s and ω of the disk. The focus of this work lies on their time dependent evolution and, therefore, it is necessary to obtain solutions for the equations (8),(16) and (18). Equations (8) and (16) can be manipulated and combined to yield decoupled equations for Σ and v_s.
Starting with eq.(16) one can regroup and partially expand the derivatives obtaining:

$$s^2\Sigma\frac{\partial\omega}{\partial t} + s^2\omega\frac{\partial\Sigma}{\partial t} + \frac{1}{s}s^2\omega\frac{\partial}{\partial s}\left(s\Sigma v_s\right) + \left(s\Sigma v_s\right)\frac{1}{s}\frac{\partial}{\partial s}\left(s^2\omega\right) - \frac{1}{s}\frac{\partial}{\partial s}\left(s^3\Sigma\nu\frac{\partial\omega}{\partial s}\right) = 0 \qquad (26)$$

Using eq.(8) one then substitutes as follows in eq.(26):

$$\frac{\partial}{\partial s}\left(s\Sigma v_s\right) = -s\frac{\partial\Sigma}{\partial t} \qquad (27)$$

and solves the result for $(s\Sigma v_s)$. This yields:

$$\frac{\left[\frac{\partial}{\partial s}\left(s^3\Sigma\nu\frac{\partial\omega}{\partial s}\right) - s^3\Sigma\frac{\partial\omega}{\partial t}\right]}{\frac{\partial}{\partial s}\left(s^2\omega\right)} = s\Sigma v_s \qquad (28)$$

from which an expression for the radial velocity v_s can be directly obtained by dividing both sides of eq.(28) by Σs. Using the result for $s\Sigma v_s$ in eq.(8) one arrives at an equation for the surface density Σ which is decoupled from v_s and only still contains the angular velocity and its derivatives in addition to Σ:

$$\frac{\partial \Sigma}{\partial t} + \frac{1}{s}\frac{\partial}{\partial s}\left[\frac{\left(\frac{\partial}{\partial s}\left(s^3 \Sigma \nu \frac{\partial \omega}{\partial s}\right) - s^3 \Sigma \frac{\partial \omega}{\partial t}\right)}{\frac{\partial}{\partial s}\left(s^2 \omega\right)}\right] = 0 \tag{29}$$

This equation is similar to a diffusion type equation for all practical purposes, although it depends on the functional form of ν. The equation contains two partial derivatives with respect to the time t, i.e. $\frac{\partial \Sigma}{\partial t}$ and $\frac{\partial \omega}{\partial t}$. While the first of these obviously only relies on local properties of the disk, the second - the derivative of ω - is linked to the global structure of the disk by eq.(18) and eq.(19). For the angular velocity to change noticeably it is therefore necessary that the whole structure of the disk change in an appreciable way. While this is a real possibility, the timescales involved in such a change, can be assumed to be considerably larger than those involved in local changes to the surface density. It therefore seems reasonable to assume, that the term $\frac{\partial \omega}{\partial t}$ will be negligible in comparison to the time derivative of the surface density. Hence, one obtains two equations that need to be solved numerically:

$$\omega(s) = \sqrt{-\frac{1}{s}\frac{\partial \Phi}{\partial s}} \tag{30}$$

and

$$\frac{\partial \Sigma}{\partial t} + \frac{1}{s}\frac{\partial}{\partial s}\left[\frac{\left(\frac{\partial}{\partial s}\left(s^3 \Sigma \nu \frac{\partial \omega}{\partial s}\right)\right)}{\frac{\partial}{\partial s}\left(s^2 \omega\right)}\right] = 0 \tag{31}$$

where the solution of eq.(30) is needed as input for eq.(31). Solving these equations iteratively, using the procedure shown in sec.(5.1.6), will yield the evolution of the parameters of the accretion disk model over time.

3 Extraneous Distributions of Matter

Accretion disks are an astrophysical phenomenon and as such they exist in the potentials created by the distributions of matter surrounding them. One of the aspects of this work is studying the time dependent evolution of massive accretion disks, i.e those surrounding supermassive blackholes, if they are placed in the background potentials created by the galaxies they reside in.
These potentials are created by the distribution of matter according to Poisson's equation - eq.(19) - with the distributions of matter consisting of several components. The major, obvious, contribution is that of the luminous matter of the host galaxy. These distributions, however, span a wide range of shapes and masses - from elliptical galaxies to spiral galaxies, from dwarfs to super massive galaxies. They, therefore, are, as a rule, not spherical, hence the potentials created by these distributions cannot be treated as constant, even if the accretion disk system is entirely "inside" such a distribution.
A lot of work has been put into potential theory and into finding potential density pairs which solve Poisson's equation, while agreeing with observed distributions of luminous matter. The results vary in complexity as one abandons assumptions of symmetry.
In addition to the distributions of luminous matter, modern physics also assumes the existence of dark matter (more in sec.(4)). These distributions must of course also be taken into account in the derivation of the background potentials. The form of these distributions is usually derived from simulations (Navarro, Frenk, & White, 1997; Eke, Navarro, & Steinmetz, 2001;Navarro et al., 2004) or from attempting to model observed effects by including a dark matter component (Hernquist, 1990; Burkert, 1995, 2000; Salucci & Burkert, 2000).

3.1 Galaxies

Obtaining a potential density pair which satisfies Poisson's equation while agreeing with observed distributions of matter has been the focus of much work in the past century and is still a topic of interest. The complexity of these pairs however varies. Some of the models make assumptions with respect to the symmetry of the systems they are meant to describe, e.g cylindrical symmetry, while others attempt a truly triaxial approach. Since the model of the accretion disk incorporates cylindrical symmetry the models used in this work to describe the host galaxies in which the systems lie embedded also display this symmetry. The size and shape of galaxies vary, with a smooth, continuous transition from spirals to ellipticals. Hence, the models used allow a certain amount of variation in their shape.

3.1.1 Spiral Galaxies

Miyamoto & Nagai (1975) have suggested a simple formulation to obtain the potential density pairs of spiral galaxies, which has the Kuzmin disks and Plummer spheroids as its limiting cases, and have shown that these or the superposition of several such potentials can give a good qualitative fit to observed potential distributions. As described by Binney & Tremaine (1987) the potential is defined as:

$$\Phi_{\mathrm{MN}}(s,z) = \frac{GM}{\sqrt{s^2 + \left(a + \sqrt{z^2+b^2}\right)^2}} \tag{32}$$

where M is the galactic mass and a and b are parameters defining the degree of deformation with the potential converging towards the spherical Plummer potential as the parameter a goes to zero:

$$\Phi_{\mathrm{MN}}(s,z) \xrightarrow{a\to 0} \Phi_{\mathrm{P}}(r) = \frac{GM}{\sqrt{r^2+b^2}} \tag{33}$$

and converging towards the extremely flattend Kuzmin disks as the parameter b goes to zero:

$$\Phi_{\mathrm{MN}}(s,z) \xrightarrow{b\to 0} \Phi_{\mathrm{K}}(s,z) = \frac{GM}{\sqrt{s^2 + (a+|z|)^2}} \tag{34}$$

Hence, this parametrization of the potential is able to produce a wide variety of potentials, depending on the choice of the parameters a and b. To obtain fits of higher quality to observed potentials, one can superimpose two or more of these potentials with different choices of the parameters, leading to a total galactic potential of the form

$$\Phi_{\mathrm{GAL}}(s,z) = \Phi_{\mathrm{MN}}(s,z,M_1,a_1,b_1) + \Phi_{\mathrm{MN}}(s,z,M_2,a_2,b_2) + \cdots \tag{35}$$

Miyamoto & Nagai (1975) have applied this prescription to the Milky Way and obtained a good fit using the superposition of two such potentials.
Obviously, it is simple to obtain the density distribution from these potentials by calculating $\Delta\Phi = 4\pi G\rho$ resulting in:

$$\rho_{\mathrm{MN}}(s,z) = \left(\frac{b^2M}{4\pi}\right) \frac{as^2 + (a+3\sqrt{z^2+b^2})(a+\sqrt{z^2+b^2})^2}{\left[s^2 + (a+\sqrt{z^2+b^2})^2\right]^{5/2} (z^2+b^2)^{3/2}} \tag{36}$$

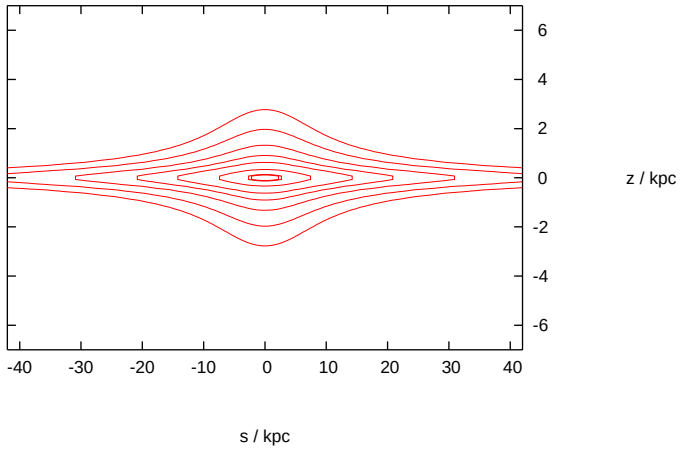

Figure 5: *Isodensity contours of the generic spiral galaxy employed in the simulations. Contour lines are scaled as multiples of the central density* ρ_{cent}*. Moving outward: 0.75, 0.3, 0.08, 0,03, 0.01, 0.003, 0.001*

This density distribution appears to be a good first order approximation to the observed distributions of spiral galaxies as shown in fig.(5).
As the interest lies on spiral galaxies in general as embedding potentials for accretion disk systems, a generic profile has been chosen with the values of the free parameters being adapted from Miyamoto & Nagai (1975).
To obtain a fairly generic spiral galaxy the parameters have been set to $a = 7$ kpc, $b = 0.3$ kpc and $M = 3 \cdot 10^{11}\ M_{\odot}$.

3.1.2 Elliptical Galaxies

While it would seem, that by simply choosing a and b correctly in eq.(32), it should be possible to obtain spheroidal potentials such as those of elliptical galaxies, Satoh (1980) has shown, that an equatorial brim remains, when using the potentials specified by Miyamoto & Nagai (1975). To solve this problem he suggested obtaining flattend higher order Plummer spheroids. Starting from the basic Plummer spheroid potential density pair given as:

$$\Phi_{\text{P}}(r) = \frac{GM}{\sqrt{r^2 + b^2}} \tag{37}$$

and

$$\rho_{\mathrm{P}}(r) = \frac{3b^2 M}{4\pi} \frac{1}{(r^2+b^2)^{\frac{5}{2}}} \tag{38}$$

with b^2 describing the inflation of the spheroid, one divides equations (37) and (38) by b^2 and differentiates the result n times with respect to its scale parameter b^2 obtaining:

$$\Phi_{\mathrm{p}}^n(r) = GM \sum_{p=0}^{n} \frac{(2p-1)!!}{(2p)!!} \frac{b^{2p}}{(r^2+b^2)^{p+0.5}} \tag{39}$$

and

$$\rho_{\mathrm{p}}^n(r) = \frac{M}{4\pi} \frac{(2n+3)!}{(2n)!!(2n+2)!!} \frac{b^{2n+2}}{(r^2+b^2)^{n+5/2}} \tag{40}$$

as the potential density pair satisfying Poisson's equation for the n-th order Plummer spheroid.
The next step towards realistic elliptical potentials is to flatten the spheroids by introducing the substitution:

$$\left(r^2+b^2\right) \longrightarrow \left(s^2 + (a+\sqrt{b^2+z^2})^2\right) \tag{41}$$

thereby replacing the spherical symmetry with a cylindrical symmetry. The potentials are then of the form:

$$\Phi_{\mathrm{p}}^n(s,z) = GM \sum_{p=0}^{n} \frac{(2p-1)!!}{(2p)!!} \frac{b^{2p}}{(s^2+(a+\sqrt{z^2+b^2})^2)^{p+0.5}} \tag{42}$$

Using eq.(19) in analogy to the method described by Satoh one obtains:

$$\begin{aligned}\rho_{\rm p}^{n}(s,z) &= \frac{M}{4\pi}\left(\frac{(2n+3)!!}{(2n)!!}\frac{b^{2n+2}[a+(z^2+b^2)^{1/2}]^2}{[s^2+(a+[z^2+b^2]^{1/2})^2]^{n+5/2}(z^2+b^2)}\right.\\ &+ \sum_{p=0}^{n}\frac{(2p-1)!!}{(2p)!!}\frac{ab^{2p+2}}{[s^2+(a+[z^2+b^2]^{1/2})^2]^{p+3/2}(z^2+b^2)^{3/2}}\\ &+ \left.\sum_{p=0}^{n-1}\frac{(2p+3)!!}{(2p)!!}\frac{b^{2p+2}[(a+(z^2+b^2)^{1/2})^2-(z^2+b^2)]}{[s^2+(a+[z^2+b^2]^{1/2})^2]^{p+5/2}(z^2+b^2)}\right)\end{aligned} \tag{43}$$

The size and appearance of the brim diminish with higher order potentials. For $n \longrightarrow \infty$ one obtains:

$$\Phi_{\rm p}^{\infty}(s,z) = \frac{GM}{(s^2+z^2+a[a+2\sqrt{z^2+b^2}])^{0.5}} \tag{44}$$

and

$$\rho_{\rm p}^{\infty}(s,z) = \frac{ab^2M}{4\pi}\frac{s^2+z^2+[a+3(z^2+b^2)^{1/2}][a+2(z^2+b^2)^{1/2}]}{[s^2+z^2+a(a+2(z^2+b^2)^{1/2})]^{5/2}(z^2+b^2)^{3/2}} \tag{45}$$

for the potential and the density respectively. As shown in fig.(6), the density distribution shows little to no brim for a more spherical aspect ratio, as is applicable for elliptical Galaxies. It therefore seems reasonable, to use this potential as a generic proxy for elliptical galaxies in which accretion disks are embedded. Since this work is focused primarily on accretion disks around super massive black holes (SMBH), and the elliptical hosts of these objects tend to be fairly large, the parameters for the generic elliptical profile have been set to $M = 1 \cdot 10^{12}\ M_{\odot}$, $a = 7$ kpc and $b = 20$ kpc.

3.2 Dark Matter

One of the goals persued here, is to compare the effects of different prescriptions of gravity on the evolution of an (embedded) accretion disk. The generally accepted model is that of General Relativity in its Newtonian limit, combined with dark matter. This scenario assumes that the luminous galaxies lie embedded in a halo composed of dark matter. The density profiles of these halos have been studied using phenomenological fits to observed

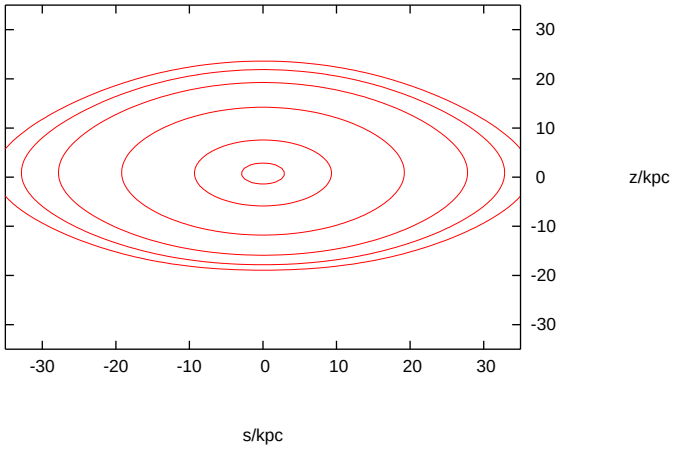

Figure 6: *Isodensity contours of the generic elliptical galaxy employed in the simulations. Contour lines are scaled as multiples of the central density* ρ_{cent}*. Moving outward: 0.75, 0.25, 0.06, 0.015, 0.008, 0.0025*

rotation curves (Burkert, 1995, 2000; Salucci & Burkert, 2000), as well as N-body simulations (Navarro, Frenk, & White 1997, henceforth NFW, Navarro et al. 2004, henceforth N04, and Eke et al. 2001, henceforth ENS). There exists, however, a discussion whether these density profiles display a central cusp, as suggested in NFW and ENS, or a central constant density core as proposed by Burkert and others (Burkert 1995 henceforth B95, Burkert 2000, Salucci & Burkert 2000). Later work by Navarro and others (N04), however, has also produced non-singular profiles.
For the simulation purposes two non-singular profiles have been selected, the B95 profile and the N04 profile, with the N04 profile being a representative of the cuspy profiles for all practical purposes.

3.2.1 The B95 Profile

Burkert has suggested a density profile for the dark matter halo, which has a core of constant density. The profile is a purely phenomenological fit, but appears to trace the dark matter density nicely (B95). This profile is given by:

$$\rho_{\rm DM}^{\rm Bur}(r) = \frac{\rho_0^{\rm Bur}(r_0^{\rm Bur})^3}{(r + r_0^{\rm Bur})(r^2 + (r_0^{\rm Bur})^2)} \tag{46}$$

where $\rho_0^{\rm Bur}$ is a constant with the dimension of a mass density and r_0^{Bur} is a scale parameter with the dimension of a length. This profile is non-singular and therefore poses no difficulties when used in the center of the halo.
Since the profile possesses spherical symmetry, its potential can be described as a monopole. For this, however, the mass contained within a radius r is needed. Using decomposition into partial fractions one obtains:

$$\begin{aligned} \rho_{\rm DM}^{\rm Bur}(r) &= \frac{\rho_0^{\rm Bur}(r_0^{\rm Bur})^3}{2(r_0^{\rm Bur})^2\,(r + r_0^{\rm Bur})} \\ &- \frac{\rho_0^{\rm Bur}(r_0^{\rm Bur})^3 r}{2(r_0^{\rm Bur})^2\,(r^2 + (r_0^{\rm Bur})^2)} \\ &+ \frac{\rho_0^{\rm Bur}(r_0^{\rm Bur})^3}{2(r_0^{\rm Bur})^2\,(r^2 + (r_0^{\rm Bur})^2)} \end{aligned} \tag{47}$$

which can be integrated without difficulty (Abramowitz & Stegun, 1972). The mass of the halo enclosed inside a radius r is then given by:

$$
\begin{aligned}
M_{\mathrm{DM}}^{\mathrm{Bur}}(r) &= \int_{V(r)} \rho_{\mathrm{DM}}^{\mathrm{Bur}}(\mathbf{r}) d^3\mathbf{r} \\
&= 4\pi \int_0^r \rho_{\mathrm{DM}}^{\mathrm{Bur}}(\tilde{r}) d\tilde{r} \\
&= M_0 \left\{ \ln\left(1 + \frac{r}{r_0^{\mathrm{Bur}}}\right) + \frac{1}{2}\ln\left(1 + \left[\frac{r}{r_0^{\mathrm{Bur}}}\right]^2\right) - \arctan\left(\frac{r}{r_0^{\mathrm{Bur}}}\right) \right\} \qquad (48)
\end{aligned}
$$

with $M_0 = 2\pi\rho_0^{\mathrm{Bur}}(r_0^{\mathrm{Bur}})^3$. This expression can subsequently be used to calculate the potential created by the dark matter halo at a given radius.
The values for the constants have been set at

$$r_0^{\mathrm{Bur}} = 3\,\mathrm{kpc} \quad \text{and} \quad \rho_0^{\mathrm{Bur}} = 0.015\ M_\odot\,\mathrm{pc}^{-3}$$

corresponding to a virial mass on the order of $10^{12}\ M_\odot$. For the ellipticals the parameters have been set to

$$r_0^{\mathrm{Bur}} = 50\,\mathrm{kpc} \quad \text{and} \quad \rho_0^{\mathrm{Bur}} = 0.01\ M_\odot\,\mathrm{pc}^{-3}$$

corresponding to a virial mass on the order of $10^{13}\ M_\odot$.

3.2.2 The N04 Profile

A different approach to the problem posed by dark matter has been adopted by various scientists. Starting from the simulation of a large, representative volume of a dark matter universe, with the parameters of the assumed cosmological model, a simulation of the evolution of matter structure in this simulation volume is run, usually to a redshift of $z = 0$. Isolated halos of the mass of interest are then selected using software routines and subsequently re-simulated at higher resolution. For a more detailed description of this method see, e.g. N04 and references therein. The results from the high resolution simulation are then spherically averaged into a numerical density profile. Rescaling these profiles leads to results implying a universal density profile (Navarro et al., 2004). Based on the assumption of a universal density profile and the simulations, Navarro et al. (2004) have introduced an empirical fitting formula that improves on previous results by Navarro et al. (1997) and Moore et al. (1999):

$$\rho_{\mathrm{DM}}^{\mathrm{N04}}(r) = \rho_{-2} \exp\left(\frac{2}{\alpha}((r/r_{-2})^{\alpha} - 1)\right) \tag{49}$$

where α is a dimensionless parameter with $\alpha \in (0.1, 0.2)$. This profile is formally non-divergent, although its behavior is very similar to that of the cuspy profiles. Use of this formula, however, requires knowledge of the scale parameters ρ_{-2} and r_{-2}. These must be calculated in some way based upon the cosmological model employed. Eke, Navarro, & Steinmetz (2001) argue that these can be derived from the characteristic concentration of the halo, which in turn is based upon the power spectrum resulting from the chosen cosmology.
With the dimension of a halo being defined by its virialized mass, i.e the mass enclosed in a sphere with an overdensity Δ times the critical density, the characteristic concentration c_{Δ} can be calculated based upon this mass and the cosmological parameters. For more detail see ENS and N04. There is a simple code available from Navarro which does this and has been used in this work. It is then very straight forward to obtain the parameters for the profile.
Starting with the virial mass M_{Δ} and:

$$M_{\Delta} = \Delta \frac{4\pi}{3} \rho_{\mathrm{crit}} r_{\Delta}^3 \tag{50}$$

with $\rho_{\mathrm{crit}} = \frac{3H^2(z)}{8\pi G}$ being the critical density for closure at a redshift z, one obtains:

$$r_{\Delta} = \left(\frac{2\, M_{\Delta}\, G}{\Delta\, H^2}\right)^{1/3} \tag{51}$$

and using $c_{\Delta} = r_{\Delta}/r_{-2}$ one arrives at the required parameter. The characteristic density can be obtained by using

$$\rho_{-2} = \Delta\, \rho_{\mathrm{crit}}\, c_{\Delta}^3 \tag{52}$$

Naturally, this profile also displays spherical symmetry, so, likewise, its potential can be treated as a monopole. However, a direct integration to obtain the enclosed mass at a given radius is not possible and an expansion followed by an analytical integration shows slow convergence, so that the enclosed mass will be calculated numerically.

The basic fact, however, remains that dark matter cannot be observed directly, but can only be inferred from e.g. the behavior of visible luminous matter or the lensing properties that can be observed. Thus one remains with indetermined profiles which must be fitted to the observed distributions. There is, therefore, a dependency upon fit parameters. While this is a condition one would hope to remedy by first principle models, it also allows for a certain lee-way, which can be practical in obtaining profiles in agreement with observations. Even the approach using cosmological N-body simulations to investigate the form of dark matter halos does not fundamentally alter the fact, that there remains a dependency upon model parameters which are only constrained to a certain extent. In the case of the N04 profile the actual model itself is an empirical fit with a free parameter and part of the uncertainty has been shifted to the uncertainty of the cosmological parameters used in the parent simulations.
This means, that no matter which approach is employed, one remains with a certain degree of uncertainty. Thus treating both models is necessary in the context of this work.

4 Generalized Gravitational Potentials

A number of astronomical observations have led to the realization, that applying the prescriptions of general relativity in its Newtonian limit to the distribution of luminous matter observed in astrophysical objects such as e.g. spiral galaxies, does not explain some of the observed behavior, the paramount example in this case, being the rotation curves of spiral galaxies. These do not decline in the expected Keplerian fashion, but show convergence toward a finite asymptotic speed of rotation. These observations have given rise to the theory of cold dark matter (CDM) halos, in which the luminous galaxies lie embedded. This model has been tested using N-body simulations to trace the evolution of a sizeable portion of the universe, including dark matter. The results of these simulations seem to agree well with the observations, however, the degree of freedom in the assumed density profile used to accurately fit the rotation curve of a spiral galaxy, has declined to such an extent, that now difficulties arise in fitting these curves.
Furthermore, while the supersymmetric extension of the standard model of elementary particles does predict particles with the required properties, to date no such candidate particle has been detected experimentally and only its gravitational effect is acessable to probe the nature of dark matter.
This is a highly unsatisfactory situation and, while dark matter is the generally accepted model, alternative theories basing on well understood physics and reasonable extrapolation thereof, which attain similar predictive and descriptive power, should also be considered and tested, if only to falsify them and learn more about the nature of dark matter.
Several such theories have been formulated, most as a modification of the Newtonian law of gravity over large length scales. These usually encounter difficulties at some stage which are related to the length-scale used. Alternatively, theories exist with an acceleration-scale which, have their own difficulties.
A main focus of the work presented here, is to study the differences in the evolution of accretion disks under the assumption of different gravitational potentials, thereby limiting the parameter space for such potentials and, if possible, finding ways of corroborating or falsifying them.

4.1 Length-Scale Modifications

Since deviations from Newtonian gravity are mainly observed on the scale of galaxies, the logical first choice for modifications of gravity is one based on a length-scale. This takes the general form:

$$F_{\text{Grav}} = F_{\text{Grav,Newt}} f(r/r_0) \tag{53}$$

Where F_{Grav} is the actual gravitational force, $F_{\text{Grav,Newt}}$ is that predicted by Newtonian theory, r_0 is a constant with the dimension of length and $f(x)$ is a function with asymp-

totic behavior:

$$f(x) = \begin{cases} 1, & \text{if } x \ll 1 \\ x, & \text{if } x \gg 1 \end{cases} \tag{54}$$

The choice for the function f, however, is not clear. One possibility is an additional $\propto \frac{1}{r}$ term, as suggested by e.g Tohline (1983) and further discussed by Kuhn & Kruglyak (1987). This would lead to the gravitational force caused by a point source taking the form:

$$F_{\text{Grav}} = -\frac{GMm}{r^2}\left(1 + \frac{r}{r_0}\right) \tag{55}$$

They stipulate a value for r_0 on the order of 15 kpc. However, there is no underlying theory based on reasonable extrapolations, that supports such a deviation.
A different approach adopted by Sanders (1984) and several times since, is that of a repulsive Yukawa term. This leads to a force of the form:

$$F_{\text{Grav}} = \frac{GMm}{r^2}\left(\frac{1}{1-\alpha}\left[1 + \alpha\left(1 + \frac{r}{r_0}\right)e^{-r/r_0}\right]\right) \tag{56}$$

Where $\alpha \approx -0.92$ and $r_0 \approx 40$ kpc. This approach can be theoretically motivated to some extent by arguing in favor of static Yukawa-like fields, that are mediated by massive bosons (Eckhardt, 1993), and would be consistent with special relativity.
However, both these modifications encounter serious difficulties when confronted with observations, as they lead to an asymptotic velocity mass relation of the form $v^2 \propto M/r_0$. This is not reconcilable with the observed Tully-Fisher relation, that states $L \propto v^4$ while it's low intrinsic scatter points to $M \propto L$. In addition these length-scale modifications are indiscernible from Newtonian gravity on the scales of the accretion disk model employed and have therefore not been implemented.

4.2 Acceleration-Scale Modifications

A different approach to the dilemma posed by the asymptotic behavior of the rotation curves of spiral galaxies, is a modification of gravity based upon an acceleration-scale. Even with the enormous masses involved, the length-scales of galactic systems are such, that the actual acceleration experienced by material due to gravity on the outskirts of a

galactic disk is minuscule. This gives rise to the possibility of introducing an acceleration-scale based modification of gravity.
In the work at hand one main focus is to study the time dependent evolution of accretion disks in modified gravitational potentials in the case of embedding. Accordingly Modified Newtonian Dynamics (MOND) suggested by Milgrom (1983) will be used as a proxy for acceleration-scale based modifications. The reason for this choice is, that MOND is the most widely discussed acceleration-scale based modification in literature and much work has been done to theoretically motivate the adhoc modification, e.g Tensor-Vector-Scalar Theory (TeVeS) as proposed by Bekenstein (2004), which is a fully covariant theory containing MONDian behavior in the correct limit, and allowing for gravitational lensing.
MOND, in the adhoc form first proposed by Milgrom, can be viewed either as a modification of inertia or gravity. While the adhoc formulation is non-relativistic and violates the conservation of momentum and angular momentum, it has been astoundingly successful in many observational tests (Sanders & McGaugh 2002 and references therein). The theoretical work done to address these issues has cast MOND in the form of a modification of gravity, as which it will be treated in this work.
MOND is based on the assumption, that below a certain acceleration the behavior of gravity departs from the standard Newtonian. The transition is gradual and parametrized by a function $\mu(x)$ which is defined by its asymptotic behavior as follows:

$$\mu(x) = \begin{cases} x, & \text{if } x \ll 1 \\ 1, & \text{if } x \gg 1 \end{cases} \tag{57}$$

Basically any continuous monotonous function with this asymptotic behavior can be used. Using this function the MOND modification in its simplest form can be formulated as:

$$\vec{\mathbf{g}_{\mathrm{n}}} = \vec{\mathbf{g}_{\mathrm{m}}} \cdot \mu\left(\frac{|\vec{\mathbf{g}_{\mathrm{m}}}|}{a_0}\right) \tag{58}$$

where $\vec{\mathbf{g}_{\mathrm{n}}}$ is the vectorial Newtonian acceleration, $\vec{\mathbf{g}_{\mathrm{m}}}$ is the actual acceleration and $a_0 \approx 10^{-8}$ cms^{-2} is a characteristic acceleration. Since $\vec{\mathbf{g}_{\mathrm{m}}}$ is given by the accelerations in the system as well as those caused by external field effects, the strong equivalence principle is broken by the prescription, while the weak formulation is preserved.
The choice of the functional form of $\mu(x)$ has only recently received restraints by the formulation of underlying theories for MOND (Bekenstein, 2004) and further comparative work (Zhao & Famaey, 2006) . However, the usual choice for $\mu(x)$ is given by:

$$\mu(x) = \frac{x}{\sqrt{1+x^2}} \longrightarrow \begin{cases} x, \text{ as } x \longrightarrow 0 \\ 1 \text{ as } x \longrightarrow \infty \end{cases} \tag{59}$$

which obviously fulfills the requirements and will be used, since MOND is being used as a proxy for acceleration scale based modifications. The Newtonian acceleration of a system is then given by:

$$\vec{\mathbf{g}_{\mathrm{n}}} = \vec{\mathbf{g}_{\mathrm{m}}} \frac{\frac{|\vec{\mathbf{g}_{\mathrm{m}}}|}{a_0}}{\sqrt{1+\left(\frac{|\vec{\mathbf{g}_{\mathrm{m}}}|}{a_0}\right)^2}} \tag{60}$$

For certain situations this expression can be further simplified. Further work on MOND by Milgrom, Bekenstein and others (Bekenstein & Milgrom, 1984; Milgrom, 1986; Sanders, 1986) has provided a non-linear Poisson equation of the form:

$$\nabla \left[\nabla\Phi \, \mu \left(\frac{|\nabla\Phi|}{a_0} \right) \right] = 4\pi G\rho \tag{61}$$

which can be used to calculate MONDian potential density pairs, although this is extremely difficult, due to the non-linear nature of the equation. However, Milgrom(1986) has shown that for most cases, especially for use in axisymmetric grid schemes, the simple prescription is an adequate approximation and only gives rise to small deviations. Since it is orders of magnitude faster than numerical solutions to eq.(61), the prescription has been used in the work presented here.

5 The Computational Model

This section is meant to clarify the actual numerical scheme used to solve the equations developed for the model in sec.(2.7), as well as to detail how the embedding of the accretion disk system and the use of generalized gravitational potentials has been implemented.

5.1 Basic Scheme

The model constructed in this work is based on the code "HTK08" written by Wolfgang J. Duschl. The actual time dependent evolution of the accretion disk hinges on solving the equations derived in sec.(2.7) numerically, starting from a well defined initial condition, i.e. an initial surface density Σ.
First of all the equations derived - eq.(30) and eq.(31) - must be discretized so that they can be treated numerically.

5.1.1 Poisson's Equation - the Law of Rotation

Having defined an initial surface density Σ and in light of the fact, that eq.(31) was derived under the assumption that the solution to Poisson's equation be known, one begins by considering eq.(30) which has the form:

$$\omega(s,t) = \sqrt{-\frac{1}{s}\frac{\partial \Phi}{\partial s}} \tag{62}$$

Obviously one must first obtain the gravitational potential Φ and then calculate its radial derivatives. This must be done using a discretization of the disk. Hence, a radial grid extending from an inner radius s_{i} to an outer radius s_{og} encompassing N gridpoints is introduced. Further an outer radius for the actual accretion disk s_{o} is specified. The disk will be set up on the inner half of the grid allowing outflow of mass from the disk without loss of that mass in the simulation. This results in a grid with:

$$s_{\mathrm{i}} = s_1 < s_2 < \cdots < s_{\frac{N}{2}-1} < s_{\frac{N}{2}} = s_{\mathrm{o}} < s_{\frac{N}{2}+1} < \cdots < s_{N-1} < s_N = s_{\mathrm{og}} \tag{63}$$

The points are chosen to be logarithmically equidistant i.e.:

$$_{10}\log(s_{\lambda+1}) \; - \; _{10}\log(s_{\lambda}) = \frac{_{10}\log(s_{\mathrm{o}}) \; - \; _{10}\log(s_{\mathrm{i}})}{N/2} \tag{64}$$

Naturally the time coordinate must also be discretized. A starting time t_b is defined and one propagates forward along the coordinate in discrete timesteps thus obtaining:

$$t_\mathrm{b} = t_1 < t_2 < t_3 < \cdots < t_l < \cdots \quad \text{where } l \in \mathbb{N} \tag{65}$$

The mass distributions contributing to the potential are the central accreting object and the accretion disk itself (the treatment of the embedding potentials will be explained in more detail later). The potential for the central monopole is well known and given by:

$$\Phi(r) = \frac{GM_\mathrm{central}}{r} \tag{66}$$

with the sign of the potential chosen in this form to insure $-(\partial\Phi/\partial s) > 0$. Since the disk is assumed to be razor thin and to coincide with the $z = 0$ plane r in eq.(66) can be replaced by s. This is valid for all other monopole like contributions as well. The potential caused by the disk is calculated using the monopole approximation, i.e. for the derivation of the potential, and only for this, the razor thin disk is treated as a spherically symmetrical distribution of matter. The potential at a given radius can then be calculated by integrating the mass enclosed within that radius and treating it as a monopole in the point of origin. While simple, this robust approximation yields results which are usually correct at least to a factor of 2 and mostly better. Using this approximation the potential can be expressed as:

$$\Phi(s) = \frac{G(M_\mathrm{central} + M_\mathrm{disk}(s))}{s} = \frac{GM_\mathrm{mp}}{s} \tag{67}$$

Once the potential is known it is straightforward to calculate the law of rotation using eq.(62). A simple finite difference scheme is used with the radial differences being smoothed using the geometrical average.

5.1.2 Evolution of Surface Density

Having thus obtained the law of rotation one can develop a scheme to discretize the time dependent evolution of the surface density:

$$\frac{\partial \Sigma}{\partial t} + \frac{1}{s}\frac{\partial}{\partial s}\left[\frac{\left(\frac{\partial}{\partial s}\left(s^3 \Sigma \nu \frac{\partial \omega}{\partial s}\right)\right)}{\frac{\partial}{\partial s}\left(s^2 \omega\right)}\right] = 0 \tag{68}$$

One can introduce the specific angular momentum $j = \omega s^2$ and a quantity $A(s,t) = s^3 \nu(s,t)\Sigma(s,t)\frac{\partial \omega(s,t)}{\partial s}$, allowing a reformulation of eq.(68) as:

$$\frac{\partial \Sigma}{\partial t} + \frac{1}{s}\frac{\partial}{\partial s}\left(\frac{\partial A}{\partial s} \Big/ \frac{\partial j}{\partial s}\right) = 0 \tag{69}$$

An explicit Lax-discretization has been chosen and implemented for $\frac{\partial \Sigma}{\partial t}$ resulting in:

$$\begin{aligned} \frac{\partial \Sigma(s_n, t_l)}{\partial t} &= \frac{\Sigma(s_n, t_{l+1}) - \frac{1}{2}\left[\Sigma(s_{n-1}, t_l) + \Sigma(s_{n+1}, l)\right]}{t_{l+1} - t_l} \\ &= \frac{\Sigma_n^{l+1} - \frac{1}{2}\left(\Sigma_{n-1}^l + \Sigma_{n+1}^l\right)}{\Delta t_{l+1}} \end{aligned} \tag{70}$$

with $\Delta t_{l+1} = t_{l+1} - t_l$. Thus the time derivative in eq.(68) has been discretized. Now the radial derivative - the second term - remains to be discretized. Having previously solved Poisson's equation, the terms involving only ω and s are known everywhere on the disk and their radial derivatives have been calculated. In analogy to Δt it then makes sense to introduce $\Delta s = s_n - s_{n-1}$. Using these derivatives one can discretize the second term as follows:

$$\begin{aligned} \frac{\partial}{\partial s}\left(\frac{\frac{\partial A(s_n,t_l)}{\partial s}}{\frac{\partial j(s_n,t_l)}{\partial s}}\right) &= \frac{\left(\frac{\partial A}{\partial s} \,/\, \frac{\partial j}{\partial s}\right)\Big|_{n+1/2}^{l} - \left(\frac{\partial A}{\partial s} \,/\, \frac{\partial j}{\partial s}\right)\Big|_{n-1/2}^{l}}{s_{n+\frac{1}{2}} - s_{n-\frac{1}{2}}} \\ &= \frac{\frac{A_{n+1}^l - A_n^l}{\Delta s_{n+1}}}{(\partial j/\partial s)_{n+\frac{1}{2}}^l \left(s_{n+\frac{1}{2}} - s_{n-\frac{1}{2}}\right)} - \frac{\frac{A_n^l - A_{n-1}^l}{\Delta s_n}}{(\partial j/\partial s)_{n-\frac{1}{2}}^l \left(s_{n+\frac{1}{2}} - s_{n-\frac{1}{2}}\right)} \\ &= \frac{A_{n+1}^l - A_n^l}{(\partial j/\partial s)_{n+\frac{1}{2}}^l \Delta s_{n+\frac{1}{2}} \Delta s_{n+1}} - \frac{A_n^l - A_{n-1}^l}{(\partial j/\partial s)_{n-\frac{1}{2}}^l \Delta s_{n+\frac{1}{2}} \Delta s_n} \end{aligned} \tag{71}$$

With these results the evolution of the surface density Σ is given by:

$$\begin{aligned}\Sigma_n^{l+1} &= \frac{1}{2}\left(\Sigma_{n+1}^l + \Sigma_{n-1}^l\right) \\ &- \frac{\Delta t_{l+1}}{s_n}\left(\frac{A_{n+1}^l - A_n^l}{\left(\partial j/\partial s\right)_{n+\frac{1}{2}}^l \Delta s_{n+\frac{1}{2}} \Delta s_{n+1}} - \frac{A_n^l - A_{n-1}^l}{\left(\partial j/\partial s\right)_{n-\frac{1}{2}}^l \Delta s_{n+\frac{1}{2}} \Delta s_n}\right)\end{aligned} \tag{72}$$

5.1.3 Radial Velocity

As the radial velocity v_s is variable and information should only propagate in causally correct directions an upwind-scheme is utilized for the simple first order derivatives of $A(s,t)$. This takes the form:

$$\frac{\partial A(s,t)}{\partial s} = \begin{cases} \frac{A_n^l - A_{n-1}^l}{\Delta s_n} & \text{if } v_s|_n^l > 0 \\ \\ \frac{A_{n+1}^l - A_n^l}{\Delta s_{n+1}} & \text{if } v_s|_n^l < 0 \end{cases} \tag{73}$$

and can be expressed in a closed form as follows:

$$\frac{\partial A(s,t)}{\partial s} = \frac{A^l_{n-\frac{1}{2}\left(sign(v_s|_n^l)-1\right)} - A^l_{n-\frac{1}{2}\left(sign(v_s|_n^l)+1\right)}}{\Delta s_{n-\frac{1}{2}\left(sign(v_s|_n^l)-1\right)}} \tag{74}$$

Using the abbreviations introduced, as well as the same simplifications with respect to $\frac{\partial \omega}{\partial t}$ eq.(28) can be simplified and reformulated to yield:

$$v_s = \frac{\frac{\partial A(s,t)}{\partial s}}{\Sigma(s,t) s \frac{\partial j(s,t)}{\partial s}} \tag{75}$$

as the expression for the radial velocity. Discretizing this expression using the upwind scheme for the radial derivative of A and the averaging scheme for j one obtains:

$$v_s\,\big|_n^l = \frac{1}{\Sigma_n^l\,(\partial j\,/\,\partial s)_n^l}\frac{A^l_{n-\frac{1}{2}\left(sign(v_s|_n^l)-1\right)} - A^l_{n-\frac{1}{2}\left(sign(v_s|_n^l)+1\right)}}{\Delta s_{n-\frac{1}{2}\left(sign(v_s|_n^l)-1\right)}} \tag{76}$$

5.1.4 Timestep - CFL

Because an explicit discretization scheme has been chosen for eq.(68), the timestep by which the system may be advanced is governed by the Courant-Friedrich-Levy condition (CFL). This condition states that in an explicit scheme the time step by which the system is advanced must fulfill:

$$\frac{v_s\,\big|_n^l\,\Delta t_{l+1}}{\Delta s_{n+\frac{1}{2}}} \leq 1 \tag{77}$$

so that the analytical domain of dependence is included in the numerical domain of dependence. Thus the time step is given by:

$$\Delta t_{l+1} \leq \min_n \frac{\Delta s_{n+\frac{1}{2}}}{v\,\big|_n^l} \tag{78}$$

since the entire grid uses one timestep and is therefore limited by the smallest one allowable.
Using these equations and this discretization scheme one can trace the time dependent evolution of the accretion disk model. However, it is still necessary to specify boundary conditions that will allow a sensible physical evolution of the system.

5.1.5 Boundary Conditions

Since in the derivation of the model equations the assumption was made, that there are no sources or sinks of mass and or angular momentum in the disk itself, it suffices to define inner and outer boundary conditions.
Material reaching the inner boundary should be able to pass over it in order to be accreted eventually. Since the processes inside s_i are not part of the model, it is expedient to assume a vanishing torque at the inner radius, allowing all material to be accreted. Since:

$$\mathfrak{G}(s_\mathrm{i},t) = 2\pi A(s_\mathrm{i},t) \quad \text{this means} \quad A(s_\mathrm{i},t) = 0 \;\; \forall \;\; t$$

leading to a choice of $\Sigma(s_\mathrm{i}, t) = 0 \quad \forall \quad t$, which would be consistent with all material reaching the inner boundary being instantaneously accreted.
Material reaching the outer edge of the grid should be able to leave the simulation unhindered, as it is far away from any other components of the system. To ensure this it is sensible to chose a constant torque at the very edge of the disk, i.e.:

$$\left(\frac{\partial \mathfrak{G}}{\partial s}\right)_{s_\mathrm{og}} = 0 \quad \text{implemented by choosing} \quad \left(\frac{\partial \Sigma}{\partial s}\right)_{s_\mathrm{og}} = 0$$

Since the outer radius of the grid is located at a very large distance from the actual disk, this is of no importance, as almost no material actually reaches the edge of the disk during the simulation time.

5.1.6 Procedure

This system of discretized equations and boundary conditions is now capable of tracing the evolution of the model accretion disk for an initial surface density and radial velocity distribution.To this end the equations are discretized and solved as detailed above. This process continues iteratively with the results being output until a predefined termination condition is reached. The schematic realization of the process is depicted below.

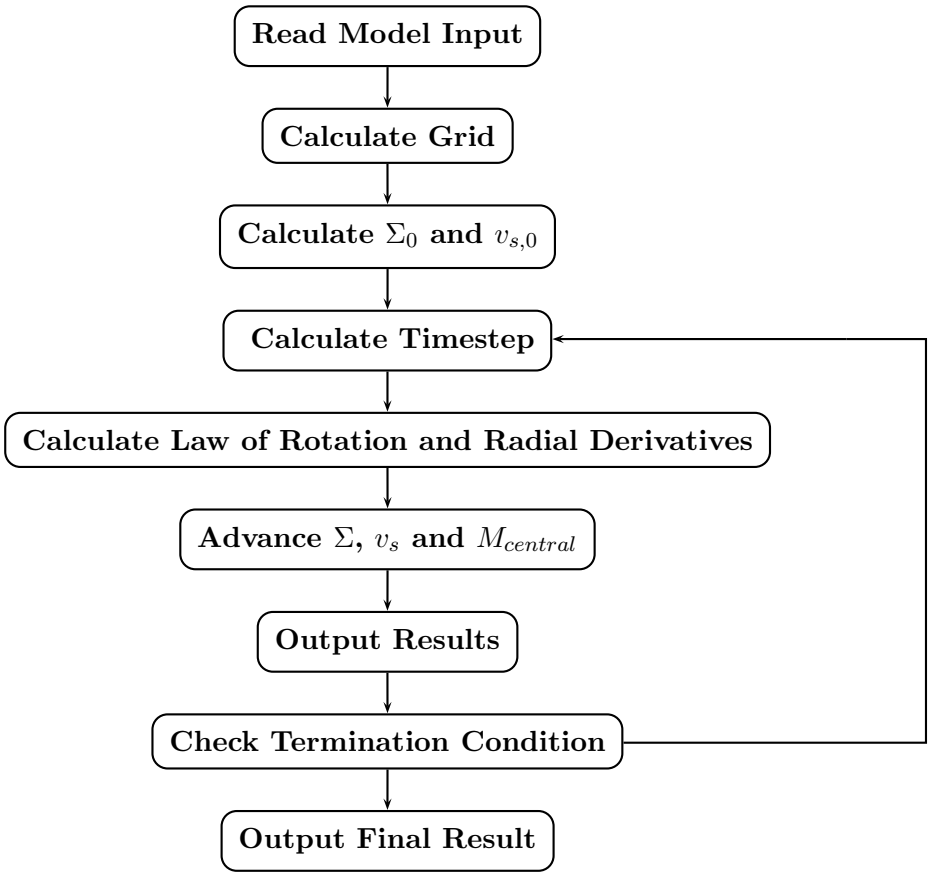

5.2 Implementation of Extraneous Distributions of Matter

Using the approach outlined, it is possible to trace the time dependent evolution of an accretion disk of varying disk and central mass. To allow a more realistic investigation, it is necessary to include the gravitational potentials generated by the surrounding distributions of matter. The mass distributions creating these additional potentials are the luminous matter of the host galaxy as well as the surrounding dark matter halo - the latter, however, only if one assumes the standard CDM model.
As described in sec.(5.1), the gravitational potential couples to the evolution of the disk via eq.(62), where it defines the law of rotation. As demonstrated, the numerical treatment of the model equations procedes in two steps. First the law of rotation is calculated using the gravitational potential and subsequently the results are used for the solution of the evolution of the surface density. Obviously, the additional gravitational background potentials will influence the law of rotation.
If one assumes, that the surface density distribution of the accretion disk does not couple to the density distributions in which it lies embedded, i.e. the evolution of the surface density of the disk does not massively influence the background potentials, it is possible

to calculate these potentials a priori and then include them in the model. This assumption is motivated by the fact that, except for the most massive disks, the total mass in the accreting system is small in comparison to the mass of the other components.
To calculate the law of rotation for the disk, one needs the gradient of the potential at the specified coordinates. Since the disk is treated as being razor thin, this means one needs to calculate the gradient of the total potential in the plane of the disk. The time dependent contribution of the disk is treated in the monopole approximation, while the other potentials are either explicitly known, e.g the Miyamoto-Nagai potential (Miyamoto & Nagai, 1975) for spiral galaxies or the Satoh potential (Satoh, 1980) for ellipticals, or can be exactly treated as monopoles because of their spherical symmetry, e.g. the B95 potential and the N04 potential.
The Poisson equation is linear allowing the total potential of the sum of the considered mass distributions contributing to be expressed as:

$$\Phi_{\text{tot}} = \Phi_{\text{disk}} + \Phi_{\text{central}} + \Phi_{\text{galaxy}} + \Phi_{\text{darkmatter}} \tag{79}$$

Using eq.(62) one obtains the law of rotation including the background potentials:

$$\omega = \sqrt{-\frac{1}{s}\frac{\partial \Phi_{\text{tot}}}{\partial s}} = \sqrt{-\frac{1}{s}\left(\frac{\partial \Phi_{\text{disk}}}{\partial s} + \frac{\partial \Phi_{\text{central}}}{\partial s} + \frac{\partial \Phi_{\text{galaxy}}}{\partial s} + \frac{\partial \Phi_{\text{darkmatter}}}{\partial s}\right)} \tag{80}$$

The computation of the derivatives is straightforward. For the terms of the monopole approximation the radial derivative in cylindrical coordinates is given as:

$$-\frac{\partial \Phi}{\partial s} = \frac{GM(s)}{s^2} \tag{81}$$

so that only the mass enclosed in a certain radius s must be calculated. To obtain the total enclosed mass inside a given radius the masses of the dark matter halo inside that radius, the ringsegments out to that radius and the central object - the black hole - are summed. This mass is then used as the monopole mass for the given radius and is of the form:

$$M_{\text{mp}}(s) = M_{\text{darkmatter}}(s) + M_{\text{disk}}(s) + M_{\text{central}} \tag{82}$$

This can then simply be plugged into eq.(81) to obtain the required derivative. Depending on which dark matter profile was used the computation of the enclosed mass varies.

5.2.1 The B95 Profile

If the B95 profile is selected, the enclosed mass at a given radius can be calculated analytically using eq.(48). This, however, poses numerical difficulties. For the inner radii the value of the term in the brace in eq.(48) is so close to zero, that it falls below machine precision and oscillates, giving no realistic results. This term has therefore been expanded to the sixth order in a Taylor expansion in powers of r/r_0^{Bur} and one obtains:

$$M_{\mathrm{DM}}^{\mathrm{Bur}}(r) = M_0 \begin{cases} \frac{2}{3}\left(\frac{r}{r_0^{\mathrm{Bur}}}\right)^3 - \frac{1}{2}\left(\frac{r}{r_0^{\mathrm{Bur}}}\right)^4 \text{, if } r/r_0^{\mathrm{Bur}} < 5 \cdot 10^{-3} \\ M_0 \left\{ ln\left(1 + \frac{r}{r_0^{\mathrm{Bur}}}\right) + \frac{1}{2} ln\left(1 + \left[\frac{r}{r_0^{\mathrm{Bur}}}\right]^2\right) - arctan\left(\frac{r}{r_0^{\mathrm{Bur}}}\right) \right\} \quad \text{, otherwise} \end{cases} \tag{83}$$

as a prescription for the computation of the enclosed mass, which is smooth to machine precision.

5.2.2 The N04 Profile

The N04 density profile on the other hand poses difficulties of its own. Since it is not possible to obtain an analytical solution for the mass enclosed in a given radius, this mass is calculated by numerically integrating the density. To do this, a linearly equidistant grid has been added inside the innermost radius of the logarithmic grid, which stretches from the center of the domain of calculation (0, 0, 0) to the inner radius of the disk. The halo mass in the center is calculated using the arithmetic mean value on this grid. For radii encompassed by the logarithmic grid a similar procedure has been used. At each grid point on the logarithmic grid an additional grid with a large number of grid points is inserted. This secondary grid encompasses an equal number of points extending from the radius associated with the gridpoint halfway to both neighboring gridpoints. An arithmetic mean density is calculated over each half and a weighted average over both means is calculated, with the weighting factors being calculated by the length of the contributing segments. Since the calculations are only performed once before the start of the simulation, the number of grid points has been chosen to be very high, i.e. on the order of 10^6.

5.2.3 Luminous Matter

The derivatives of the potential created by the surrounding luminous galaxy, on the other hand can be expressed analytically and calculated directly. If eq.(32) is differentiated with respect to s one obtains:

$$-\frac{\partial \Phi_{\mathrm{MN}}}{\partial s} = \frac{GMs}{\left(s^2 + (a+b)^2\right)^{3/2}} \tag{84}$$

Analogously one obtains the radial derivative of the Satoh potential:

$$-\frac{\partial \Phi_{\mathrm{p}}^{\infty}}{\partial s} = \frac{GMs}{\left(s^2 + a(a+2b)\right)^{3/2}} \tag{85}$$

In both cases the derivatives have been calculated in the s,ϕ-plane, that is to say at coordinates (s, ϕ, 0). This is also the only component of the total gradient, which is present in the plane of the disk under the assumptions made. These expressions are then plugged back into eq.(80) to obtain the total derivative and thereby the law of rotation.

5.3 Implementation of Generalizations of Gravitational Potentials

The implementation of the MOND prescription for gravity follows the simple modification first suggested by Milgrom (1983). First the Newtonian gravitational acceleration is calculated for the chosen distribution of luminous matter. This is done as described in sec.(5.2), but only the acceleration, not the law of rotation, is calculated. Given the symmetry of the problem eq.(60) can be further simplified and formulated more explicitly:

$$\begin{aligned} g_{\mathrm{n}} &= g_{\mathrm{m}} \cdot \mu\left(\frac{|g_{\mathrm{m}}|}{a_0}\right) \\ &= \frac{g_{\mathrm{m}}^2}{\sqrt{a_0^2 + g_{\mathrm{m}}^2}} \end{aligned} \tag{86}$$

This is a biquadratic equation from which g_{m} can be determined as:

$$g_{\mathrm{m}} = \left(\frac{1}{2} g_{\mathrm{n}} \left(g_{\mathrm{n}} + \sqrt{g_{\mathrm{n}}^2 + 4a_0^2}\right)\right)^{1/2} \tag{87}$$

Using eq.(87) and the Newtonian acceleration g_{m} is calculated and used to subsequently calculate the law of rotation according to:

$$\omega = \sqrt{\frac{1}{s} g(s)} \tag{88}$$

which is an equivalent formulation to eq.(80). The rest of the program runs as for the Newtonian prescription.

6 Results

The model detailed and motivated above has been used to attempt to do preliminary investigations into several questions concerning accretion disks. First of all the influence of background potentials, such as those caused by the luminous host galaxy and a putative dark matter halo, on the time dependent evolution of the accretion disk has been studied for various accreting systems. Secondly the influence of modifications to Newtonian gravity on the evolution has been tested and compared with the results for the standard ΛCDM model. Finally attempts have been made to investigate whether these systems can be used to discern between different models of gravity or place constraints on the possible alternatives to the cold dark matter model.
To these ends models spanning a black hole mass range of $10^5 M_\odot$ - $10^9 M_\odot$ and a disk mass range of $10^7 M_\odot$ - $10^{10} M_\odot$ were simulated in all embedding scenarios. A representative selection of the results obtained is presented here.

Nomenclature

The work presented here bases on contrasting various embedding scenarios, which nevertheless remain similar to some extent. It is necessary at times, to plot a variety of different embedding scenarios simultaneously, to be able to discern the relevant differences. To this end the models must be distinguishable. To facilitate this and to be able to name and identify models in a manageable form, the following nomenclature will be employed where not specifically stated otherwise.
First the logarithm to the base 10 of the initial black hole mass in units of $M_\odot$ will be stated, preceded by a B. This will be followed by the logarithm to the base 10 of the initial disk mass in units of $M_\odot$ preceded by a D. Thus a system consisting of a $10^6 M_\odot$ black hole and a $10^8 M_\odot$ disk will be referred to as B6D8.
This system can be embedded either in the generic spiral galaxy potential, the generic elliptical galaxy potential or not at all. In the case of no embedding the name will remain as stated. For a system embedded in a spiral galaxy the suffix Sp will be added, and in the case of an elliptical galaxy as embedding potential the suffix E will be added.
In addition to being embedded in a galactic potential the system can also reside in a dark matter halo with a constant density core, denoted by the suffix B95, or in a quasi-cuspy dark matter halo profile, denoted by the suffix N04. Depending on the gravity prescription used, the models will have the suffixes NEWT for Newtonian models or MOND for MONDian models. However, for reasons of brevity, the NEWT suffix is omitted at times, for models with Newtonian gravity.
Consequently a system consisting of a $10^6 M_\odot$ black hole and a $10^8 M_\odot$ disk embedded in a spiral galaxy potential and a N04 dark matter halo will be referred to as B6D8SpN04 or B6D8SpN04NEWT and the same disk system embedded in a spiral galaxy using MONDian gravity will be referred to as B6D8SpMOND.

6.1 Preliminary Investigations and Model Parameters

For the investigations conducted a logarithmic grid was used. The number of points on this grid was set at 30, since no substantial gain is derived from a finer grid, as shown for the grids with 50 and 100 points respectively, fig.(7). The choice is necessitated by the fact that a large parameter space must be covered, with simulations running over 10^{10} years. This choice of resolution keeps the time required for simulations reasonable; a 30 gridpoint simulation runs approximately 6 hours, while a 50 gridpoint simulation is more in the vicinity of 11 hours. Furthermore, the physical resolution of the simulation is intrinsically limited by the assumption of a razor thin disk. This assumption basically reduces the attainable physical resolution to distances on the order of $h(s)/s$, with $h(s)$ being the height of the disk at the radius s, giving an absolute upper limit for the amount of gridpoints that can be meaningfully employed. This is on the order of $O(10^2)$ gridpoints. Given the convergence visible, this upperlimit, and the time consideration, the choice of 30 gridpoints appears justified.
In addition, the parameter β for the β-viscosity (sec.(2.3) & Duschl et al. (2000)) has been set to the value $\beta = 0.001$ in concurrence with the turbulence experiments cited earlier. The accretion efficiency has been set to 0.1 in accordance with the estimates presented in Frank, King, & Raine (2002) and the inner radius of the disk has been set at 10^{15} cm with the truncation radius at 10^{20} cm. This choice was made to render the results comparable, however, it should be mentioned that for the most massive black holes, i.e. those with $10^9 M_\odot$, this distance is equivalent to about 3 Schwarzschild radii, so that the results for the innermost regions of the most massive disks might be subject to other physical effects and be different from those calculated here. However, since the focus of interest lies primarily on the outer regions, the choice should be valid.

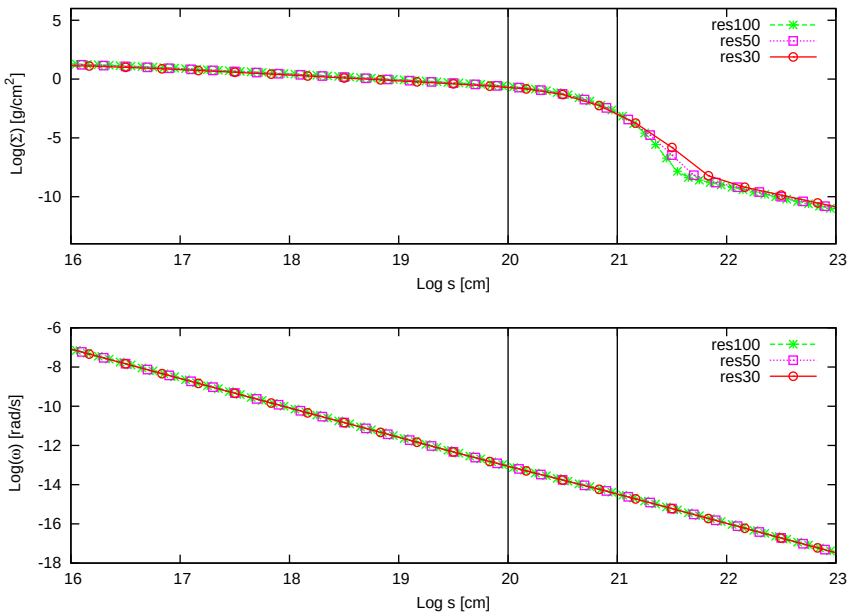

Figure 7: *Surface Density (top) and angular velocity (bottom) over disk radius for a grid with 30 points, 50 points and 100 points. The disk model used is a* $10^6 M_\odot$ *BH with a* $10^8 M_\odot$ *disk. The resolution obtained improves with the number of points in the grid, however, the results for 30 gridpoints are reasonable and the calculation time is the shortest, so this resolution has been chosen for the parameter space studies. The vertical line at* 10^{20} *cm marks the initial outer radius of the disk. The line at* 10^{21} *cm* ≈ 320 *pc is an orientation guide. The results remain physically relevant to this radius and somewhat beyond.*

6.2 Embedding Circumnuclear Disks

As stated, one of the main goals of this work, is to discern the influence of embedding potentials on the evolution of accretion disk systems located therein. To quantify the effects of embedding, comparison with the non-embedded case is necessary. Simulations of accretion disk systems covering a range of central and disk masses have been run as references for the embedding scenarios. As can be seen in figures (8) and (9), the systems evolve to a relaxed state with near Keplerian rotation and a stable surface density profile which is depleted over time. The radial velocities show the expected inflow onto the SMBH at the inner edge and the outflow coupled with the transport of angular momentum at the outer edge. As can be seen the systems develop self-similar solutions which scale with the disk and central mass but all retain the same functional form. The surface density is defined by the mass of the disk as can be seen in fig.(8) with the mass of the central black hole (BH) having no discernible effect. The angular velocity is dominated by the central black hole, with the lowest mass BH leading to the smallest angular velocities, fig(8). There is a trend visible towards larger angular velocities for larger central masses. Within this trend larger disk masses respectively also lead to larger angular velocities. The only outlier on this trend is the constellation of a $10^5 M_\odot$ BH with a $10^9 M_\odot$ disk. This, however, can most likely be explained by the employed monopole approximation, which creates a larger effective central mass very rapidly.

The same behavior is visible in the radial velocity and the viscous timescale. Since the viscous timescale is related to the angular velocity as $\tau_{\text{visc}} \propto \omega^{-1}$ the systems of lesser mass also have longer viscous timescales. The resultant larger viscosity also allows for greater outflow rates from the edge of the disk. The extent of the influence of the BH can clearly be seen in the radial velocity, with the outlier behavior of the $M_{\text{BH}} = 10^5 M_\odot$, $M_{\text{Disk}} = 10^9 M_\odot$ system clearly visible.

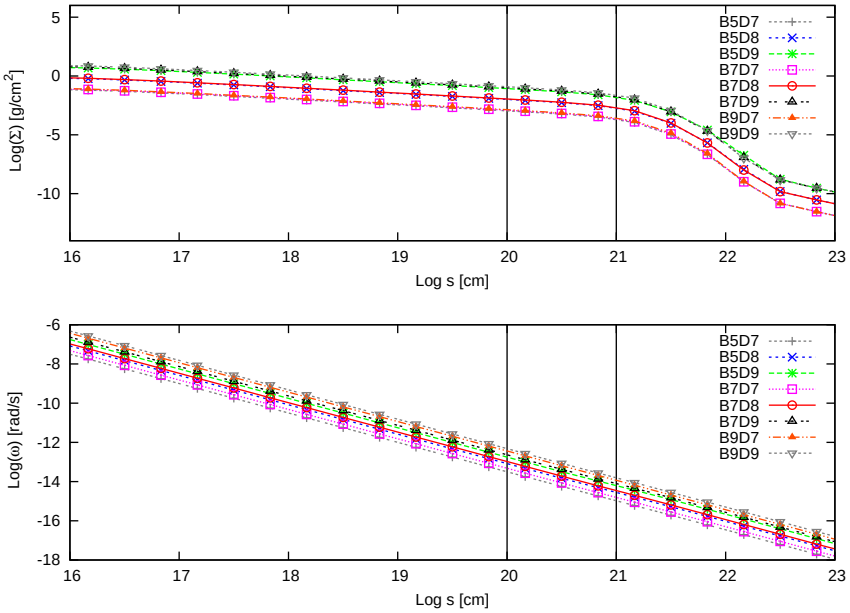

Figure 8: *Surface density (top) and angular velocity (bottom) over disk radius for various combinations of disk mass and BH mass. The upper panel shows the dependency of the surface density on the initial disk mass with negligible effect from the BH. The lower panel shows the basic dependency of the angular velocity on the BH mass being modified by the disk mass. The model B5D9 shows different behavior, which is probably due to the monopole approximation for the disk self-gravity. A self-similarity is visible in the solutions, scaling with the mass of the system.*

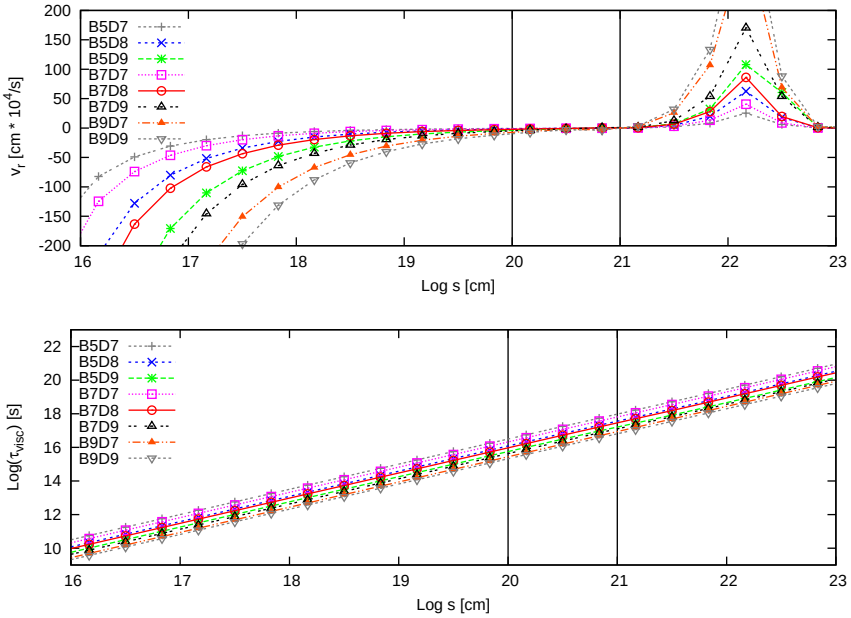

Figure 9: *Radial velocity (top) and viscous timescale (bottom) over disk radius for the same models as in fig.(8). The larger extent of the influence of a more massive BH is visible in the radial velocity profiles, with larger masses leading to greater infall velocities at a given radial distance. This equates to a larger outflow rate, driven by the larger viscosity of more massive systems. The behavior of the B5D9 model in these plots also fits with the explanation of a large effective monopole.*

6.2.1 Luminous Host Galaxies

To discern the effect of a luminous host galaxy on the evolution of the accretion disk, the reference scenarios were combined with the host potentials described. The potential of the host galaxy gives rise to an additional inward acceleration, which affects the flow of material in the disk. As can be seen in fig.(12) and fig.(13) the outflow of material is reduced in comparison to the non-embedded case. This additional acceleration also confines the disk to smaller radii and steepens the truncation of the disk as is visible in fig.(10) and fig.(11), also leading to a higher surface density. However, the effect of the embedding potential is dependent upon the mass of the disk system. Low mass systems, such as that consisting of a $10^5 M_\odot$ BH and a $10^7 M_\odot$ disk, as well as the one containing a $10^7 M_\odot$ BH and a $10^7 M_\odot$, disk are influenced more by the effect, than larger mass systems. In these systems the potential caused by the disk and the central BH dominate the total potential to much larger radii, as becomes clear by looking at the radial velocities, so the difference only becomes noticeable farther outward. The degeneracy in the dependency of the surface density upon the mass of the central object (see fig.(8)) is broken by embedding. Evidence for this is the extent of the disk with a $10^9 M_\odot$ BH and a $10^7 M_\odot$ disk, in comparison to those systems of similar disk mass, but smaller central masses, as shown in fig.(10) and fig.(11). The surface density remains similar to its non-embedded profile to a much larger distance, before being affected. This effect is less visible, but also relevant, for larger disk masses, with the system containing a $10^9 M_\odot$ BH and a $10^9 M_\odot$ disk being the least constrained. The dependency of the influence upon the system mass is also visible in the angular velocity profile, depicted in the bottom panel of fig.(10) and fig(11). The angular velocity is dominated by the embedding potential at a radial distance of about 10^{21}cm. The lower mass disks are dominated earlier showing deviations from their non embedded behavior, while the high mask disks show an almost smooth transition with little to no deviations. It remains to be said, that the B5D9 model also shows the previously discussed behavior in the embedded scenario.
Although the embedding leads to a breaking of the degeneracy of the surface density and the angular velocity becomes dominated by embedding effects at large radial distances, the self-similarity of the solutions, as well as their convergence to a relaxed quasi-stationary state, remains basically unaffected.
It should be noted at this point, that, in the case of embedding, the results obtained begin to loose physical relevance at radial distances on the order of 10^{22} cm. Such a radial distance corresponds to 3.2 kpc and it is unlikely that the central accretion disk extends to such distances in the form used in this model. However, results out to 10^{21} cm (320 pc) and somewhat beyond can be seen as being of physical relevance.

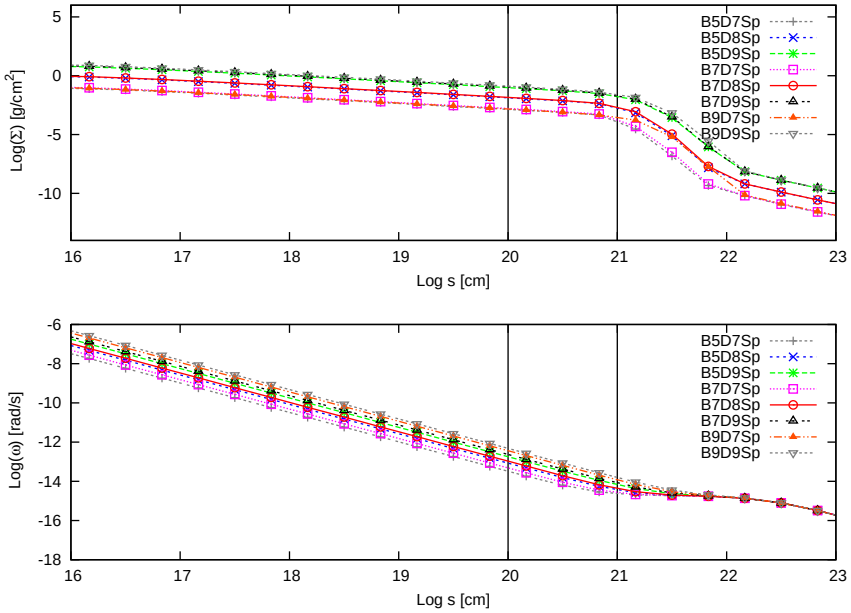

Figure 10: *Surface density profile (top) and angular velocity (bottom) over radial distance for various disk systems embedded in a generic spiral galaxy potential with* $M_{\rm Gal} = 3 \cdot 10^{11} M_\odot$ *and scale parameters chosen to* $a = 7$ *kpc and* $b = 0.3$ *kpc. The degeneracy in the dependence of the surface density upon the central BH mass is broken, as can be seen clearly for the models B5D7Sp B7D7Sp and B9D7Sp. The truncation of the disk is steeper than shown in fig.(8), with especially the low mass disks being constrained to smaller radii by the additional inward-directed acceleration, caused by the embedding potential. The varying degree in dominance of the potential depending on the mass of the system is also apparent in the angular velocity profile, with the behavior at large radii being dominated by the embedding and the shape of the transition being defined by the mass of the system components. The larger the system mass, the smaller the deviation. Nevertheless, the solutions remain self-similar.*

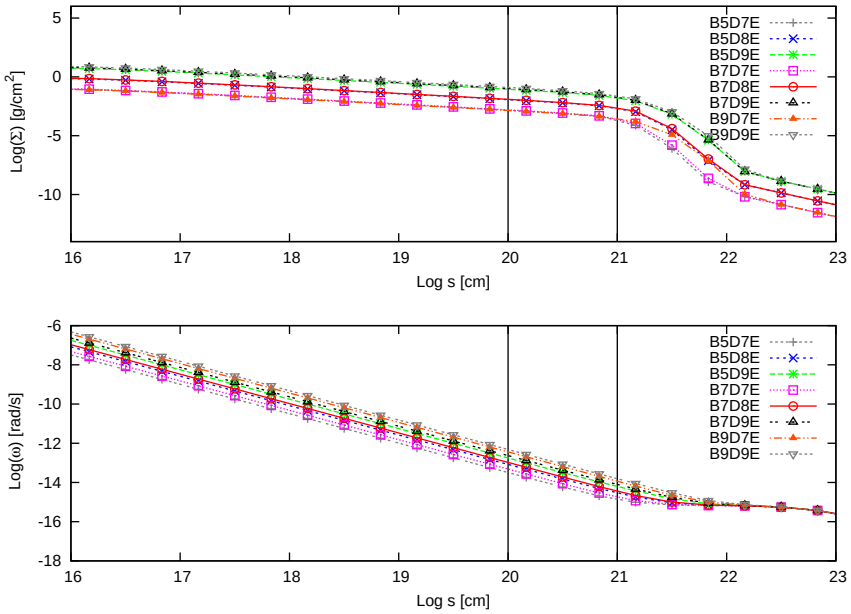

Figure 11: *Surface density (top) and angular velocity (bottom) over radial distance for the same disk systems as in fig.(10), embedded in a an elliptical galaxy with* $M_{\mathrm{Gal}} = 10^{12} M_{\odot}$ *and scale parameters* $a = 7$ *kpc and* $b = 20$ *kpc. The same behavior as in the case of spiral embedding is visible. However, the asymptotic angular velocity is slightly lower and the point of dominance of the galactic potential lies at a greater radial distance than for the spiral galaxy. This infers a somewhat smaller enclosed mass.*

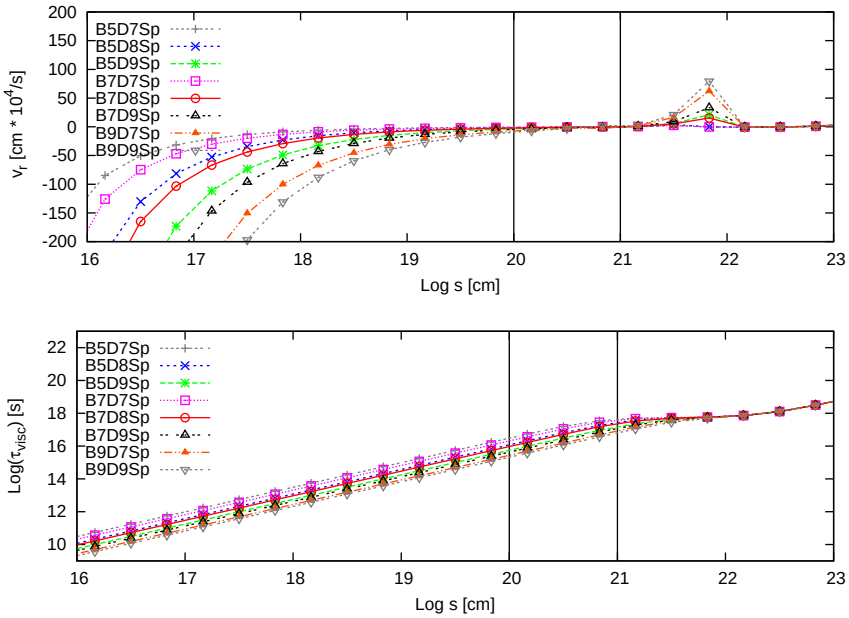

Figure 12: *Radial velocity (top) and viscous timescale (bottom) over radial distance for the same disk systems as in fig.(10), in the same spiral galaxy potential. The influence of the embedding potential on the radial velocity is especially clear in the outflow characteristics. The speed of the outflow has been drastically reduced in comparison to the non-embedded scenario. This corresponds to the constraint of the disk to smaller radii, as shown in fig.(10). The outflow rate remains the highest for massive system with large viscosities, declining to the lowest mass systems. The viscous time-scale shows that, as in the case of no embedding, the most massive systems develop the fastest. Also, the extent of the influence of the disk system components is visible in the radial velocity profile, agreeing with the small deviations observed for massive systems.*

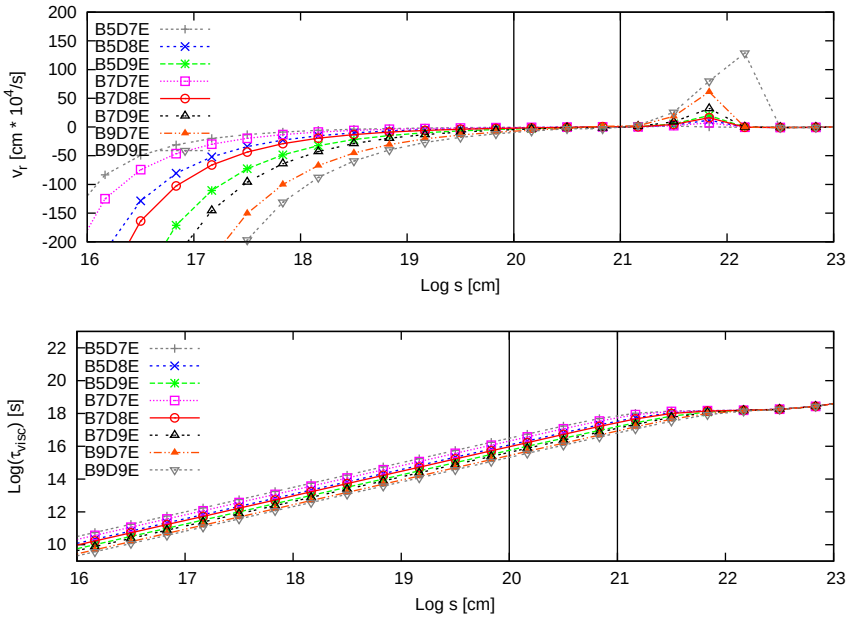

Figure 13: *Radial velocity (top) and viscous time-scale (bottom) for the same systems as in fig.(12), embedded in an elliptical potential. The behavior of the profiles shows the same systematic response to embedding in the physically relevant regions, as in the case of spiral galaxies.*

Comparison of Spirals and Ellipticals

It is noteworthy, that the profiles of the disk properties behave so similarly, even down to the numerical values, in each of the embedding scenarios. While there are small differences, as can be seen in fig.(14) and fig.(15), the similarity is striking. This is explained by the fact, that the disk system resides in the central most part of the galaxy. In the spiral galaxy, this is the so called bulge, which has a density distribution that very closely resembles an elliptical one. Additionally, although the generic elliptical galaxy has a larger mass than the generic spiral galaxy, $10^{13} M_{\odot}$ in comparison to $10^{12} M_{\odot}$, the larger scale lengths of the elliptical galaxy lead to a very similar central density for both scenarios, a fact which is in agreement with observations. As can be seen in fig.(14) the angular velocity is actually somewhat lower for the elliptical scenario and the dominance of the galactic potential sets in at slightly larger distances, inferring a smaller enclosed mass. However, this should not be seen as a fundamental result, but as the result of trying to use a “generic“ galactic potential. It, therefore, appears that the type of host galaxy is of lesser importance for the development of the accretion disk system.

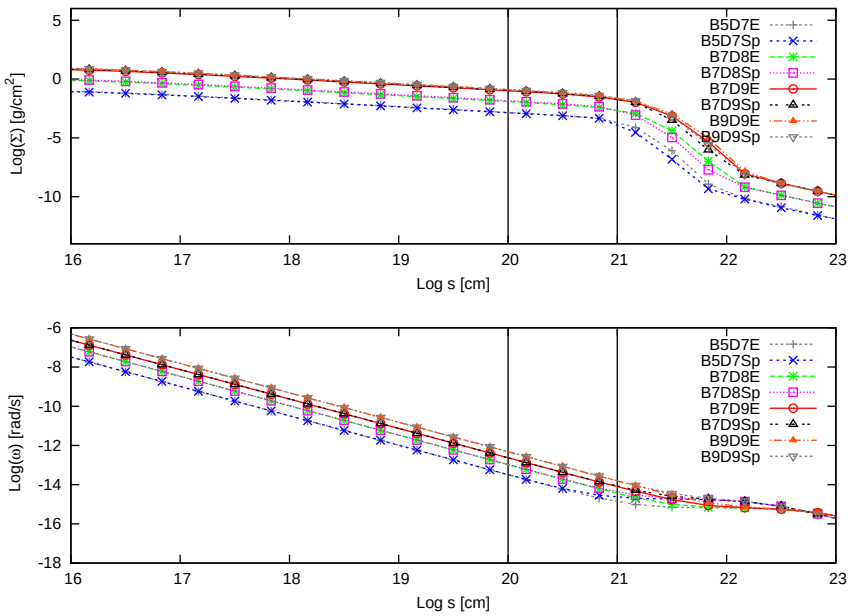

Figure 14: *A direct comparison of the surface density and angular velocity profiles for spiral and elliptical host galaxies. The response of the profiles to embedding is basically identical for both scenarios. The somewhat larger enclosed mass inside the relevant region in the case of spiral embedding, leads to the radial extent of the disk being slightly more constrained and the angular velocity being dominated by the galactic potential at a smaller radius and to a larger value for the velocity. Nevertheless, the profiles are basically self-similar and it appears that the type of host is of little importance for the evolution of the central disk system, under the assumptions made.*

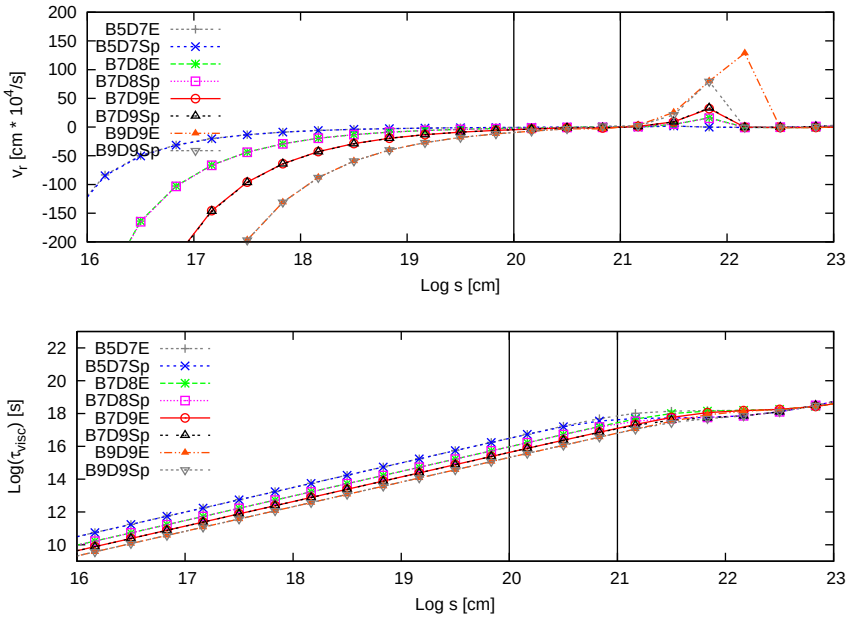

Figure 15: *A direct comparison of the radial velocity and viscous time-scale for both scenarios, as in fig.(14). These profiles also show the same development in both cases, with the smaller enclosed mass in the elliptical case resulting in a slightly larger viscous time-scale at the outer edge of the system.*

6.2.2 Luminous Host Galaxies & Dark Matter Halos

AGN not only lie embedded in the potentials created by their luminous hosts, but also in such potentials, as are created by the dark matter halos (DMH), in which the host galaxies themselves reside. In the literature there is a debate, whether these profiles are cuspy, i.e have a divergent density towards their center, or posses a core of constant density. These are the two basic scenarios for spherically symmetrical profiles. The problem has been addressed by numerical simulations, but the resolution remains extremely poor inside the central kpc. Both models have been implemented to investigate the intrinsic evolution differences they create. Both dark matter halo profiles used to embed spiral galaxies are based on a virial mass of $10^{12} M_{\odot}$, while those used to embed ellipticals are based on a virial mass of $10^{13} M_{\odot}$.

The N04 Dark Matter Halo

Fig.(16) shows the surface density and angular velocity profiles for various disk systems, embedded in the generic spiral galaxy potential and a N04 DMH with a virial mass of $10^{12} M_{\odot}$. The N04 profile is cuspy for all practical purposes and leads to a large effective monopole mass. The system obviously diverges from the evolution seen, when only embedded in a galaxy potential. As is the case for the galactic potential, the DMH constrains the disk to smaller radii, however, the larger effective monopole increases the viscosity, allowing the system to transport more mass to larger radii. This smooths the truncation of the disk. The angular velocity is dominated by the halo at a much smaller radial distance and raised considerably. These effects are also visible in the radial velocity, which shows a significant increase at the innermost resolved radii and the much shorter viscous time-scale for larger radii, fig.(17). The smoothing of the disk truncation is especially effective for the lower mass systems, as the self-gravity is relatively smaller, in comparison with the potential created by the DMH. This leads to a more gradual outflow and lower radial velocities at the disks edge.

Fig.(18) and fig.(19) show that the behavior of the profiles is basically identical in the relevant regions for the embedding scenarios using an elliptical host. This result agrees with the greater importance of the halo for the evolution of the disk at comparatively smaller radial distances. Due to the scaling relation of the halo, the larger virial mass results in a very similar central density, since the extent of the halo is larger. These effects suppresses the small deviations visible in fig.(14)

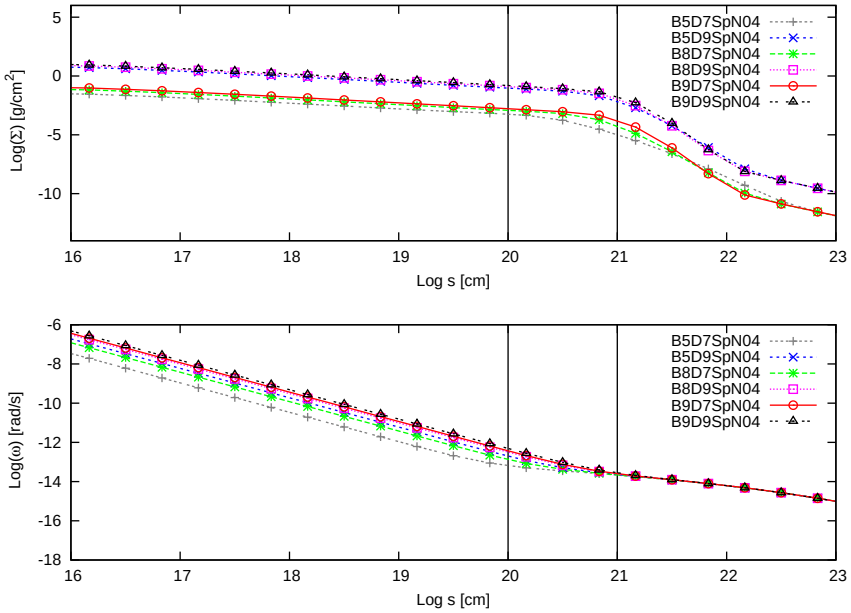

Figure 16: *Surface density (top) and angular velocity (bottom) over radial distance for various disk systems in a spiral galaxy potential with a N04 dark matter halo profile. The quasi-cuspyness of the profile leads to a large central dark matter mass. Since the profile is spherically symmetrical, this is added to the monopole contribution, resulting in a large effective monopole. This constrains the disk, as is the case for galactic potentials. However, the viscosity is enlarged, allowing more material to be shifted outward, leading to a softening of the disks truncation.*

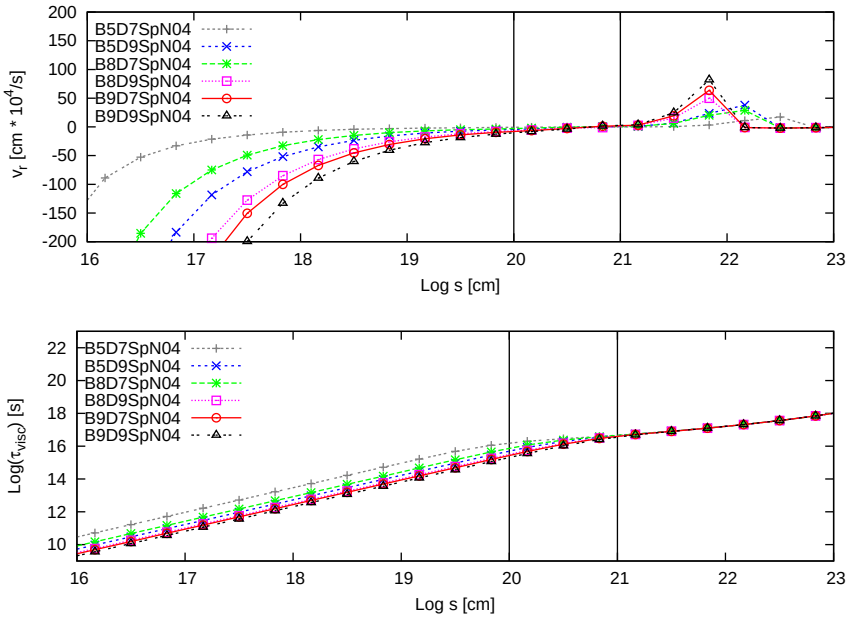

Figure 17: *Radial velocity (top) and viscous time-scale (bottom) over radial distance for the same scenarios as in fig.(16). The larger effective monopole mass leads to a larger viscosity and a shorter viscous time-scale. The softening of the truncation of the disk can be seen in the radial velocity profile, with the outflow velocities rising in a more gradual manner, especially for the lower mass disks. The larger mass systems remain more dominated by their self-gravity, making the effect less notable.*

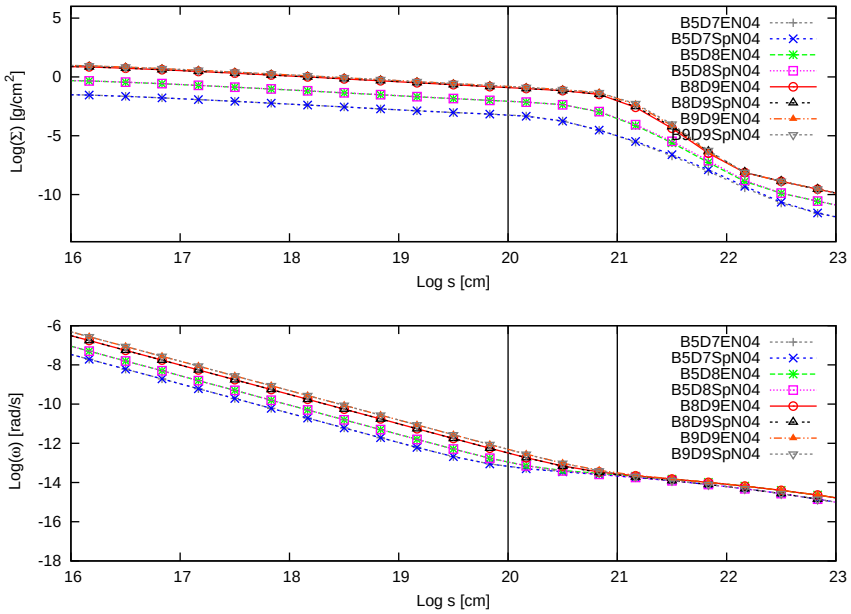

Figure 18: *Direct comparison of elliptical and spiral embedding scenarios, in the respectively relevant N04 halo. The potential of the systems is dominated at such a radiu, that the deviations seen in fig.(14) are suppressed. The profiles appear identical over the entire physically relevant radial extent. The evolution of the disk systems and the processes involved therein, are independent of the type of host galaxy in this embedding scenario.*

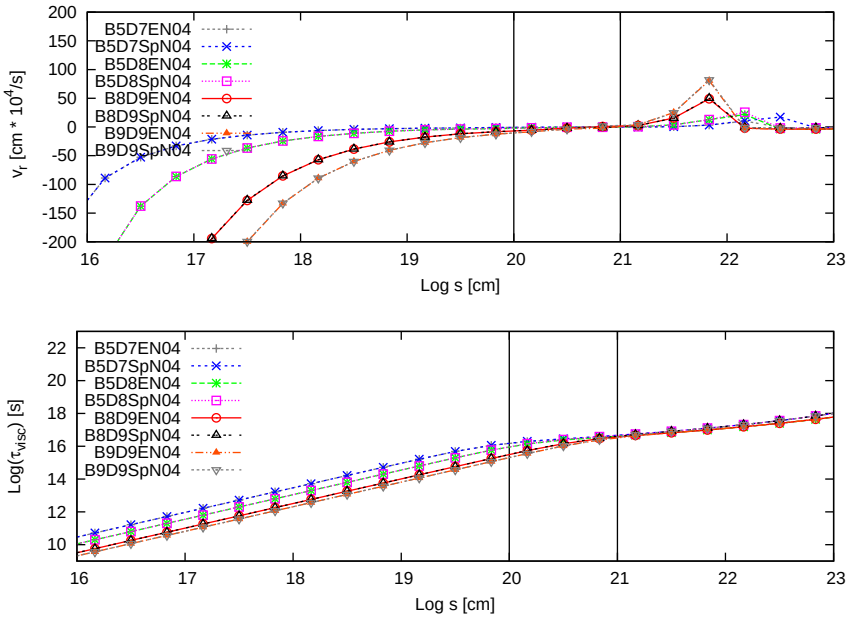

Figure 19: *Direct comparison of radial velocity and viscous time-scale for both host systems in their respective N04 halos. The profiles are nearly identical over the whole relevant radial extent, with the only deviation occurring at the very edge of the physical domain for the lowest mass system. The low mass of the system can be seen as being utterly dominated by the halo and galactic potentials at this distance. The slightly smaller enclosed mass of the galaxy might then lead to a smaller constraint, allowing a greater outflow. It remains, however, that since "generic" galaxies have been used, the results are identical within reasonable margins.*

The B95 Dark Matter Halo

The B95 DMH has a constant density core. Fig.(20) shows the surface density and the angular velocity for a B95 DMH, with a virial mass of $10^{12} M_{\odot}$ and a generic spiral galaxy and Fig.(21) shows the radial velocities and viscous time-scales. There is no discernable difference to the behavior, shown by the disk systems embedded solely in the galactic potential, since the cumulative mass of the halo is dominated by the disk system and the galactic potential at the relevant radial distances. This can also be seen in fig.(22), which shows a direct comparison of the surface density and angular velocity of various disk systems, embedded in an elliptical potential, with and without a B95 halo.

Due to the lack of influence of the B95 halo on even the lowest mass systems, the results of the comparison of embedding in elliptical and spiral potentials remain unaltered.

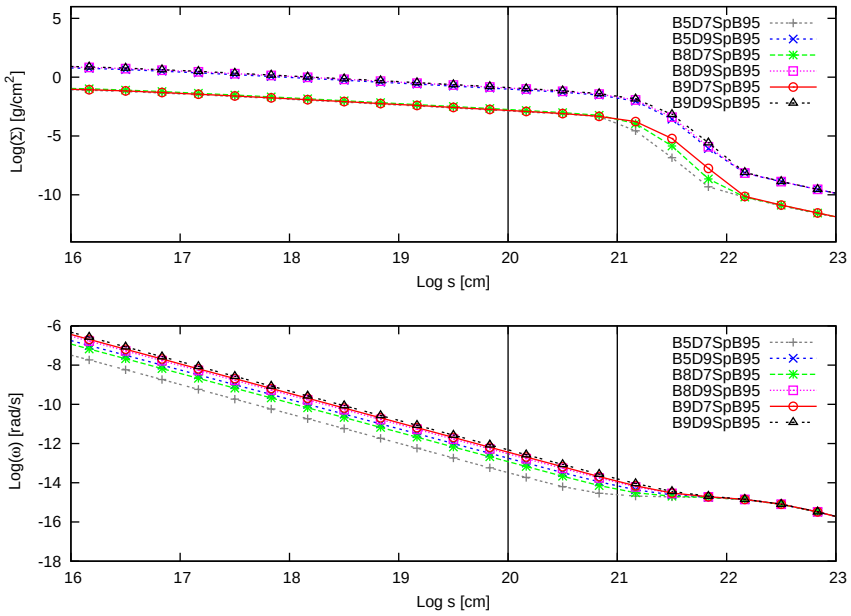

Figure 20: *Surface density (top) and angular velocity (bottom) over radial distance for various disk systems embedded in a spiral galaxy and a B95 dark matter halo. The effect of the constant density core profile halo is negligible and the dynamics of the system are dominated by the disk itself and by the luminous matter distribution at the outer edge of the disk.*

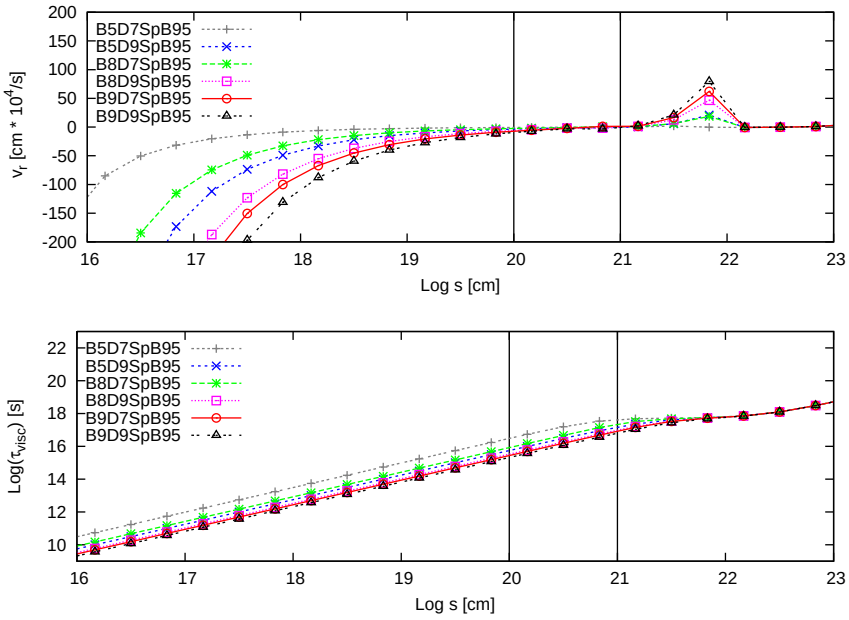

Figure 21: *Radial velocity (top) and viscous timescale (bottom) for the same scenarios as in fig.(20). The behavior is the same as that of systems, embedded solely in a luminous galactic potential. The constant density core does not contribute enough mass density in the innermost regions, to have a discernable effect.*

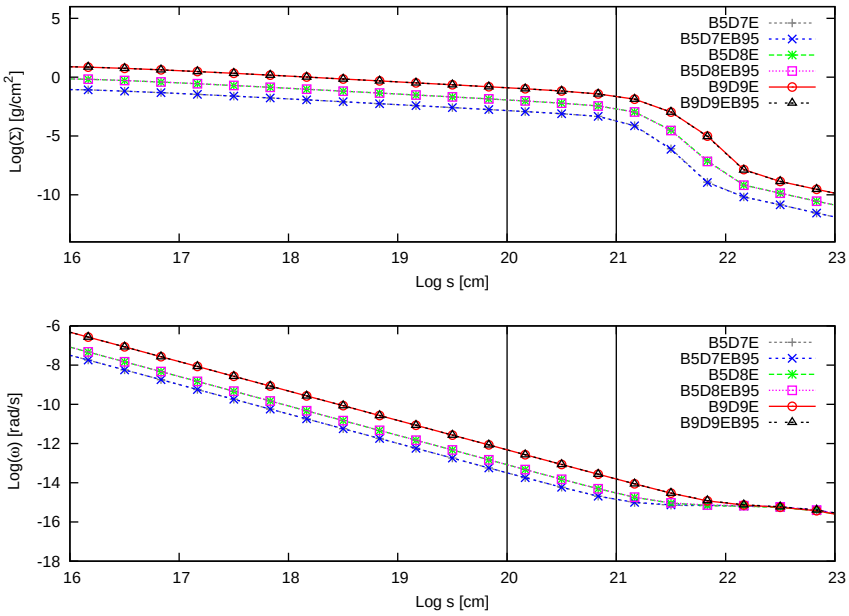

Figure 22: *Surface density and angular velocity for various disk systems in an elliptical host with and without a B95 halo. The halo has no discernible influence on the profiles. This is also the the case for spiral galaxies. The discussion of the influence of the host type can be referred to the embedding scenarios using only galactic potentials.*

Even though the embedding of the disk systems in background potentials causes differences in their evolution, the evolution of different disk systems in the same embedding scenario remains self-similar, as can bee seen in fig.(16), fig.(17), fig.(20) and fig.(21). Fig.(18) and fig.(22), show that this is the case for both studied luminous host potentials, and that the form of the luminous host is of little to no importance.

Fig.(23) and fig.(24), as well fig.(25) and fig.(26), show a comparison of treated embedding scenarios for spiral galaxies, for a disk system with a $10^5 M_\odot$ BH and a $10^8 M_\odot$ disk and two different disk systems, respectively. The constraining of the disk to smaller radii as well as the larger angular velocities, and the effects mentioned above caused by the larger viscosity, are clearly visible, showing that, while the central solutions for disk systems are not strongly affected by embedding, the behavior at their edges is influenced to a greater or lesser extent by the background potentials in which they reside, depending upon the system mass.

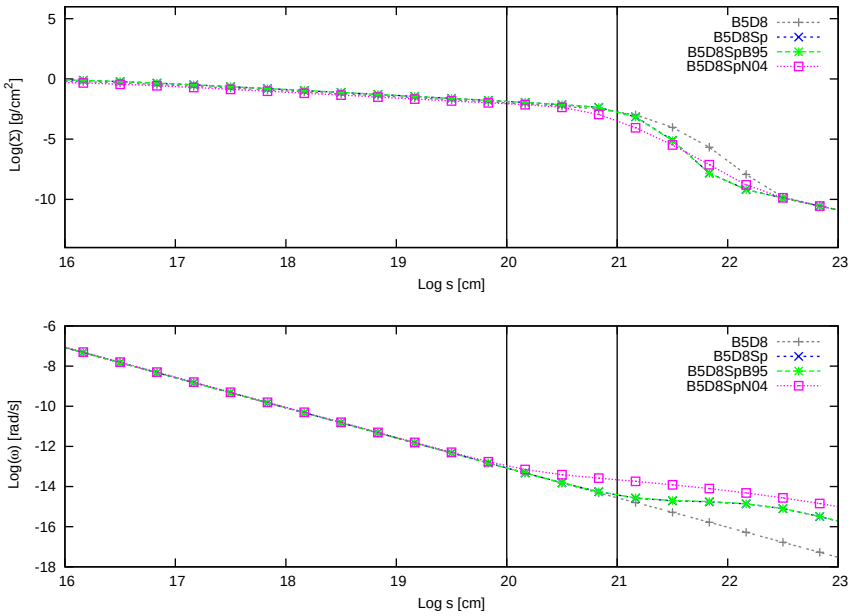

Figure 23: *Surface density and angular velocity over radial distance for a* $10^5 M_\odot$ *BH and a* $10^8 M_\odot$ *disk. The system is shown non-embedded, with only a spiral potential added, in a spiral potential with a B95 DMH, and in a spiral with a N04 DMH. Both DMH are based on a virial mass of* $10^{12} M_\odot$*. The disk is constrained to smaller radii by embedding potentials. The larger effective monopole and larger viscosity in the N04 case lead to a softening of the truncation at the disks edge in comparison to the B95 and spiral galaxy only case, which are degenerate. The angular velocity profile shows a large difference in the angular velocities at* 10^{21} *cm, clearly distinguishing between a cuspy profile and one with a constant density core.*

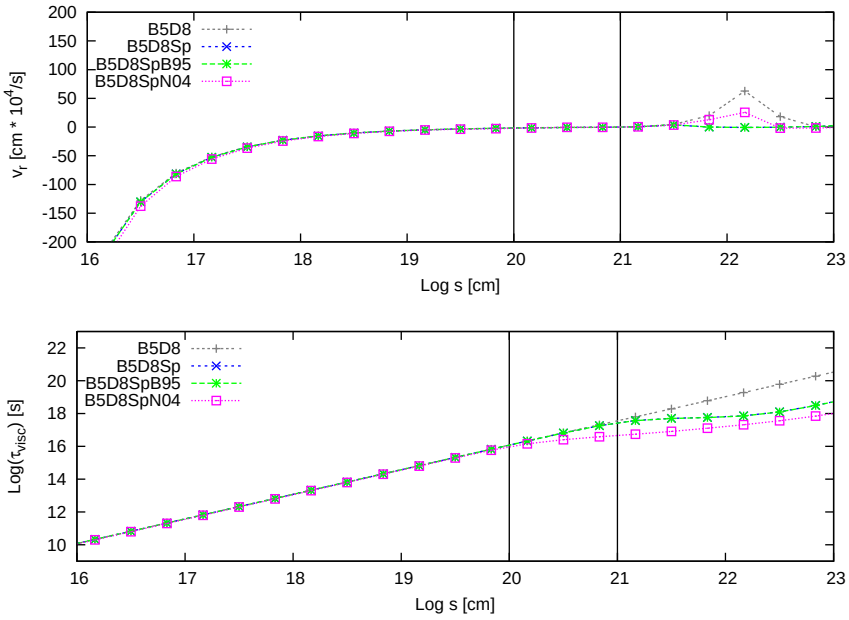

Figure 24: *Radial velocity and viscous time-scale for the systems as shown in fig.(23). The effect of the cuspy dark matter profile, even at small radii, can be seen in the radial velocity profile, with the inflow speed being larger than in other embedding scenarios. The larger viscosity due to the N04 halo also allows for a greater outflow and hence a more rapid evolution of the disk.*

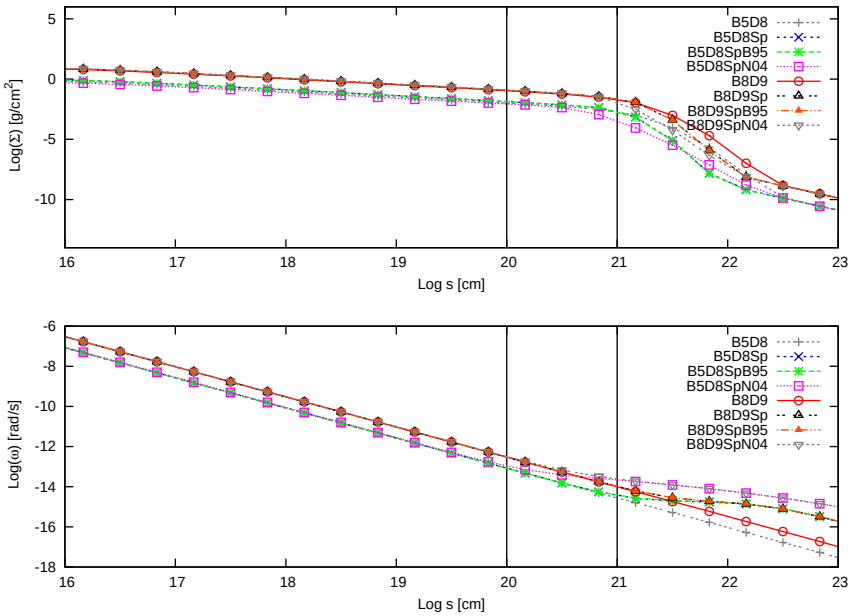

Figure 25: *Same as fig.(23), but with two disk systems. The second system is a* $10^8 M_\odot$ *BH and a* $10^9 M_\odot$ *disk, a system much more dominated by self-gravity than the lower mass system. The effects of the N04 embedding are clearly visible in both systems, as well as the degeneracy for the constant density core halo profile. The dominance of the halo mass contribution to the potential sets in at larger radii for the larger mass system. The profiles remain self-similar in each of the embedding scenarios, while showing strong differences at the disk edge for different scenarios.*

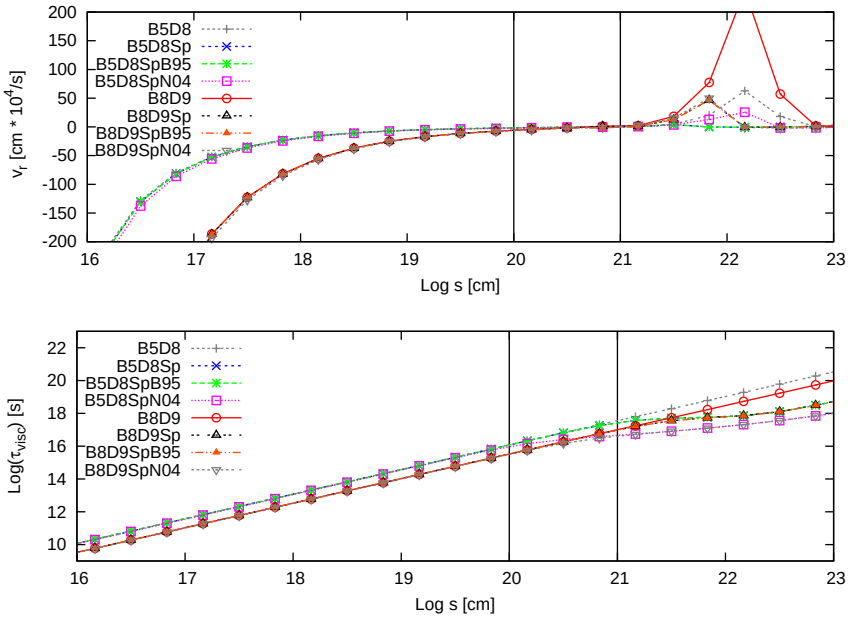

Figure 26: *Radial velocity and viscous time-scale for the systems depicted in fig.(25). The effect of the embedding halo is larger for low mass systems, since the contribution is relatively larger in comparison to the disk system itself. This can be seen in the radial velocity profile at small as well as large radii. The large radii show a more gradual, but greater outflow velocity for low mass systems, while the large mass systems show little to no difference in outflow velocity. The behavior of the viscous timescale is congruent with a larger viscosity.*

Self-similarity and Evolution Time

The solutions for the surface density, the velocity profile and the viscous time-scale are self-similar, at least in the context of an embedding scenario. The values for the surface density and the extent of the disk scale with the mass of the system, but the basic shape of the profile remains the same (see previously presented results). This means that the dynamic evolution of these systems is similar, even though they span a large range in mass.
The systems evolve towards a quasi-stationary state, in which they continue their evolution by simply depleting the disk. It is of interest after what time these systems reach the quasi-stationary state. The simulations show (fig.(27) and fig.(28) that the evolution time depends on the mass of the system. The larger the central mass in a disk system is, the faster it can develop and accrete. The same is true for the disk mass itself, with larger mass systems developing more rapidly than lower mass systems. The central mass, however, is of slightly greater importance than the disk mass for the evolution time of a system. Additionally, the simulations show that embedding increases the speed of the evolution, especially for low mass systems, and that this increase is also dependent upon the effective additional mass. These results agree well with the hypothesis that SMBH can grow in AGN and with the observations showing that high mass SMBH reach the peak in their number density earlier than lower mass SMBH, also known as anti-hierarchical growth.

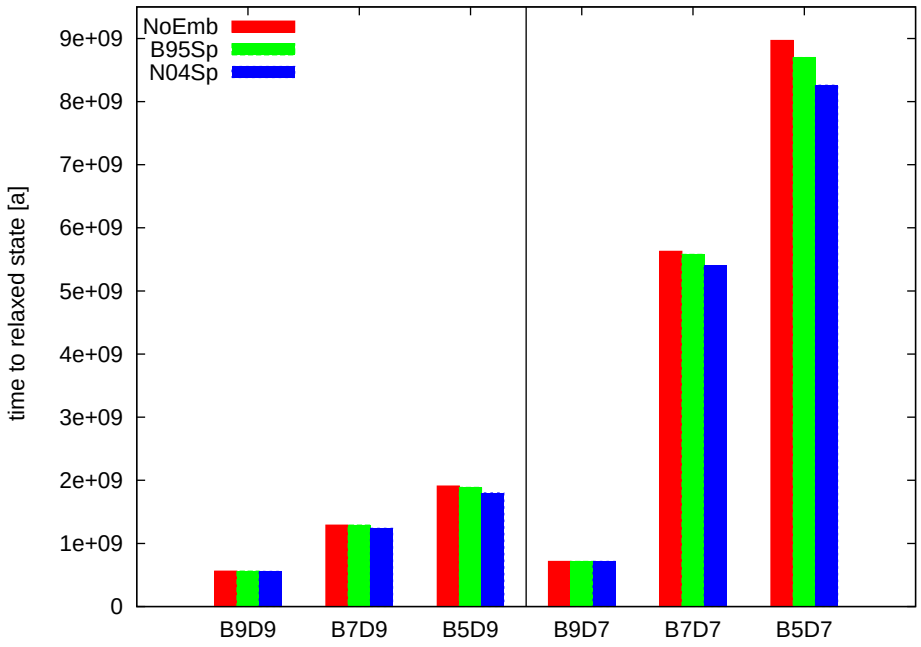

Figure 27: *Evolution time to a comparable quasi-stationary state for several disk systems in different embedding scenarios in years. The bars show B9D9, B9D7, B7D9, B7D7, B5D9 and B5D7 systems without further embedding (red), in a spiral potential with a B95 halo (green) and in a spiral potential with a N04 halo (blue). The dependency of the evolution time on the mass can easily be seen. The greater importance of the central mass is visible in the comparison between the B9D7 and B7D9 systems. Embedding shortens the evolution time of low mass systems. The results comply with anti-hierarchical growth scenarios.*

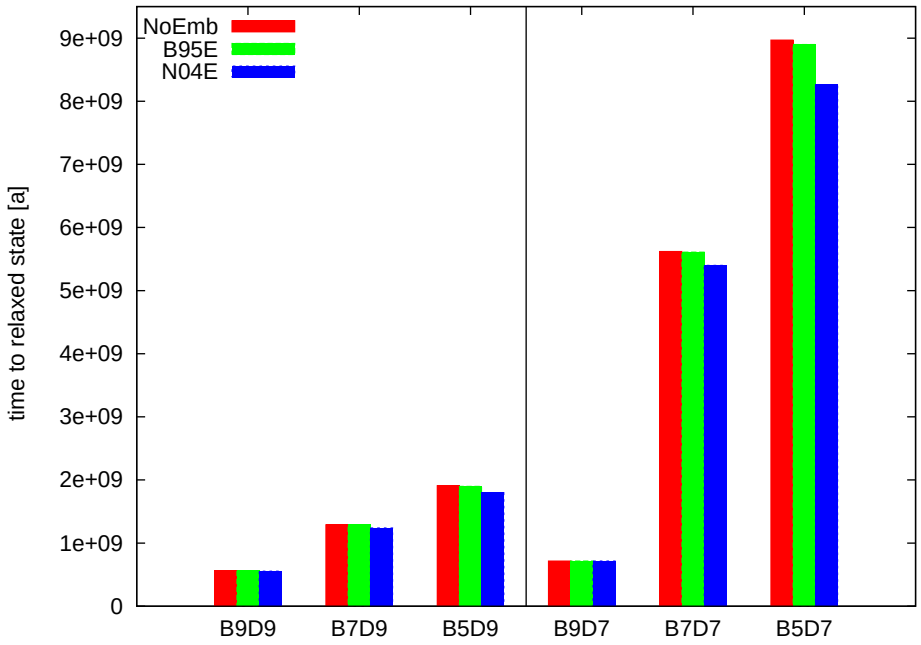

Figure 28: *Evolution time to a comparable quasi-stationary state for several disk systems in different embedding scenarios in years. The bars show B9D9, B7D9, B5D9, B9D7, B7D7 and B5D7 systems without further embedding (red), in an elliptical potential with a B95 halo (green) and in an elliptical potential with a N04 halo (blue). The dependency of the evolution time on the mass can easily be seen. The results are similar to those of spiral embedding, however the effect of the galactic embedding is somewhat smaller, due to the smaller enclosed mass. The importance of mass for the evolution time can be seen in the smaller difference in evolution time between the B5D7, B5D7EB95 systems and the B7D7, B7D7EB95 systems respectively, in comparison to the equivalent spiral systems in fig.(27), where the larger enclosed mass leads to a greater difference. The results comply with anti-hierarchical growth scenarios and demonstrate the dominant importance of disk system parameters for the evolution time.*

6.3 Effects of Generalized Potentials

All of the simulations described in the previous sections have been run using Newtonian gravity with dark matter halos. A second focus of this work is, to study the effects of an acceleration based modification to Newtonian gravity and contrast them with the Newtonian results. Hence, the relevant scenarios are a CDM embedding scenario using Newtonian gravity, versus the same combination of disk system and luminous galaxy with the MOND prescription for gravity.
The previous section has shown, that the different dark matter halo profiles lead to very different results for the evolution of the disk. Thus, differentiating between these two scenarios might be possible. Both of these must be compared with MOND as a proxy for acceleration based modifications. Given the fact that MOND is only effective in the weak field limit, the extent of the gravitational influence of the disk system is important.

Fig.(29) and fig.(30), show the surface density, angular velocity, radial velocity and viscous time-scale for a high mass and a low mass model embedded in a spiral potential using both CDM scenarios and a MOND scenario. The results for the cuspy N04 profile can easily be distinguished from the B95 profile and are valid for both luminous host types as previously shown. However, the MOND model is nearly identical to the B95 model, especially in surface density and angular velocity, the two quantities which can best be observed, as shown in fig.(31). This is also the case for the elliptical scenario, although there are slightly larger differences in angular velocity and surface density visible (fig.(32) than for the spiral case.

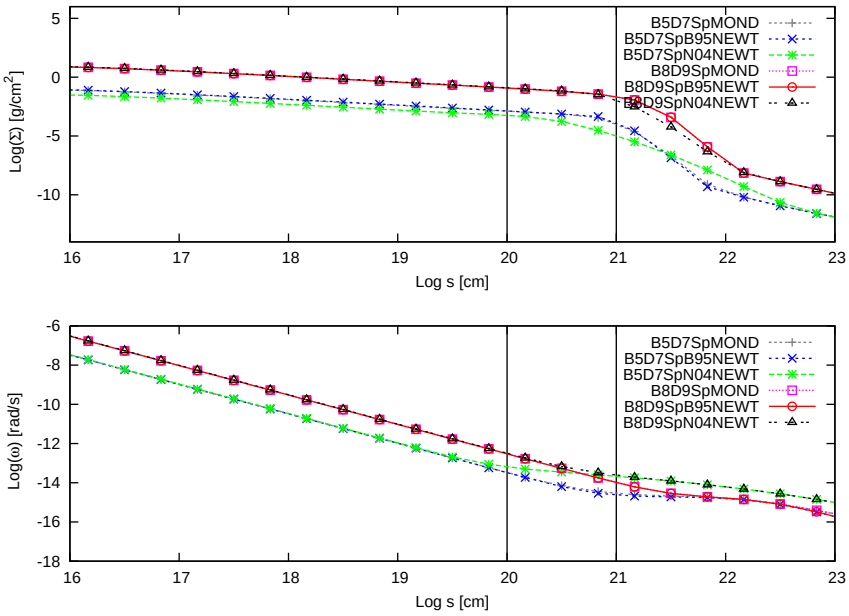

Figure 29: *Surface density and angular velocity for a high mass and a low mass disk system (standard nomenclature) embedded in a generic spiral galaxy potential with Newtonian gravity and a N04 DMH, with Newtonian gravity and a B95 DMH and MOND gravity. The N04 profile is easily distinguishable, while the B95 and MOND scenarios seem largely identical.*

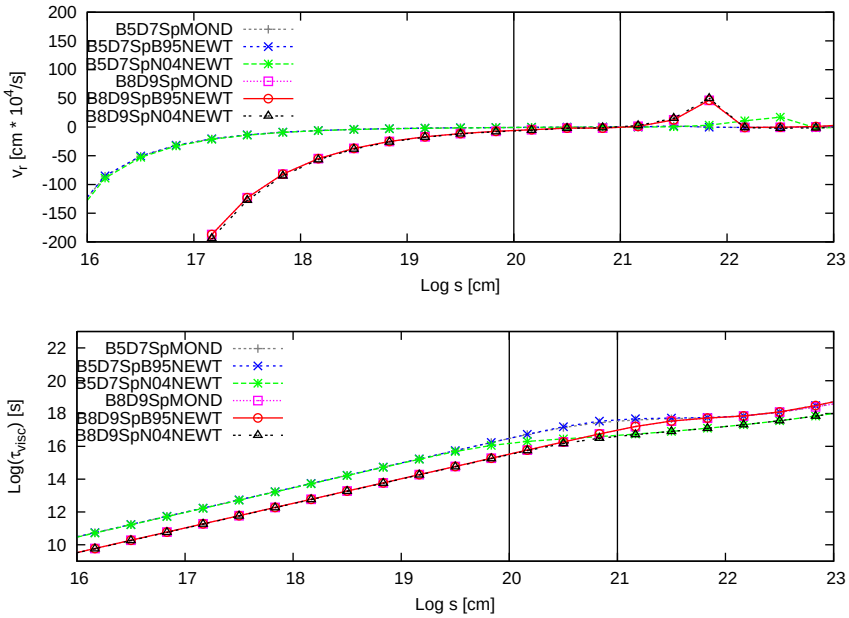

Figure 30: *Radial velocity and viscous time-scale for a high mass and a low mass disk system (standard nomenclature) embedded in a generic spiral galaxy potential with Newtonian gravity and a N04 DMH, with Newtonian gravity and a B95 DMH and MOND gravity. The N04 profile is easily distinguishable, while the B95 and MOND scenarios seem largely identical.*

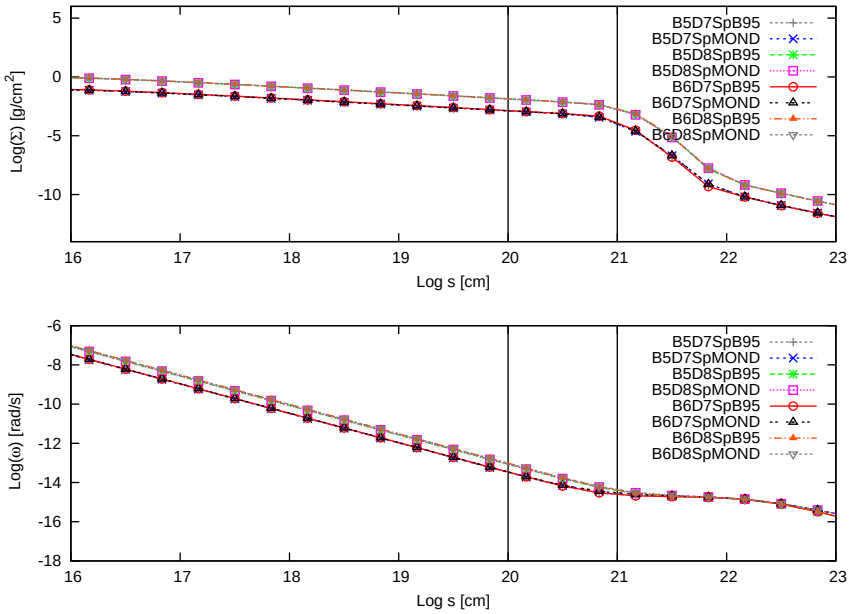

Figure 31: *Surface density and angular velocity for low mass disk systems ($10^5 M_\odot$ and $10^6 M_\odot$ BH with $10^7 M_\odot$ and $10^8 M_\odot$ disks) embedded in a spiral galaxy potential, using B95 dark matter halos and MOND gravity modification respectively. The systems appear almost identical. Only a small difference can be observed in the angular velocity at the edge of the disk for the lowest mass systems.*

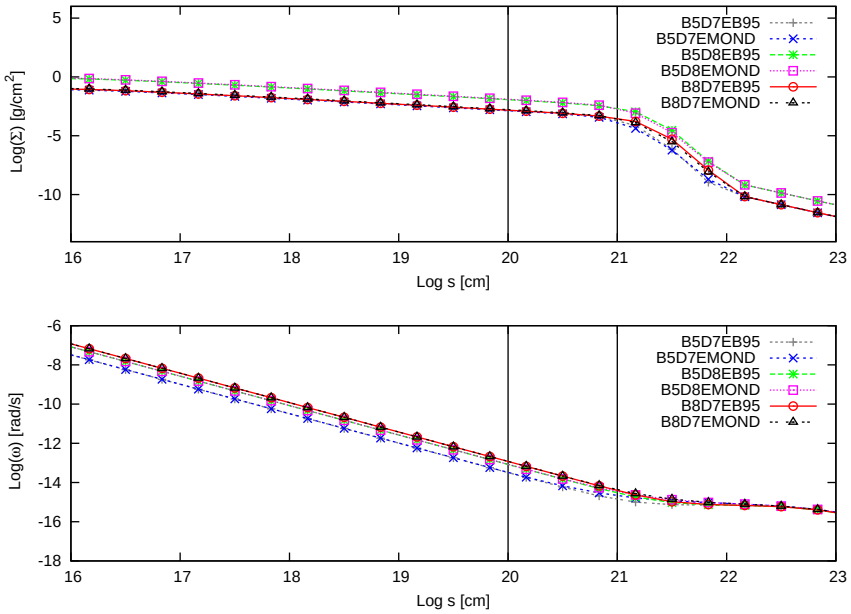

Figure 32: *Surface density and angular velocity for low mass systems ($10^5 M_\odot$ and $10^8 M_\odot$ BH with $10^7 M_\odot$ and $10^8 M_\odot$ disks) embedded in an elliptical galaxy potential, using B95 dark matter halos and MOND respectively. The systems appear almost identical as in the case of spiral embedding, however, there is a somewhat larger discrepancy in the angular velocities of the lowest mass disk systems at the edge of the disk.*

Careful examination of the angular velocity profile for the lowest mass systems, however, shows that the angular velocities differ at large radii, before the system is dominated by the embedding potential of the galaxy, fig.(33). The larger effective gravitational acceleration, caused by the modification, leads to a larger angular velocity than the almost negligible constant density core CDM profile.
The somewhat smaller enclosed mass in the elliptical scenario places the systems edge deeper in the MOND regime than in the spiral galaxy embedding. As a result the differences in angular velocity are larger, since the discrepancy between the Newtonian and the modified gravitational acceleration is larger as shown in fig.(34).

A radial distance of 10^{21} cm is equivalent to 320 pc. At this distance the actual rotational velocities $v_\phi = \omega s$ for the disk systems encompassing a $10^5 M_\odot$ or $10^6 M_\odot$ BH and a $10^7 M_\odot$ disk are 30.2 kms^{-1} for the MOND scenario and 25.11 kms^{-1} for the B95 scenarios with a spiral potential. This would result in a Doppler shift difference of

$$\frac{\Delta\Lambda}{\Lambda} = 1.7 \cdot 10^{-5}$$

on the edge of what might be observable, even though the low surface density poses a dilemma for the flux from this region. As shown in fig.(33), this difference in angular velocity decreases rapidly with growing system mass, and is not present for large mass systems, as they do not enter the weak field regime far enough to demonstrate MONDian behavior.
Although the difference is slightly larger in the case of an elliptical potential of the form used here, it is unlikely that such a phenomenon will be observed, since the disk systems in such larger elliptical galaxies are usually more massive than those in spiral galaxies, and are thus less likely to lie in the MOND regime.

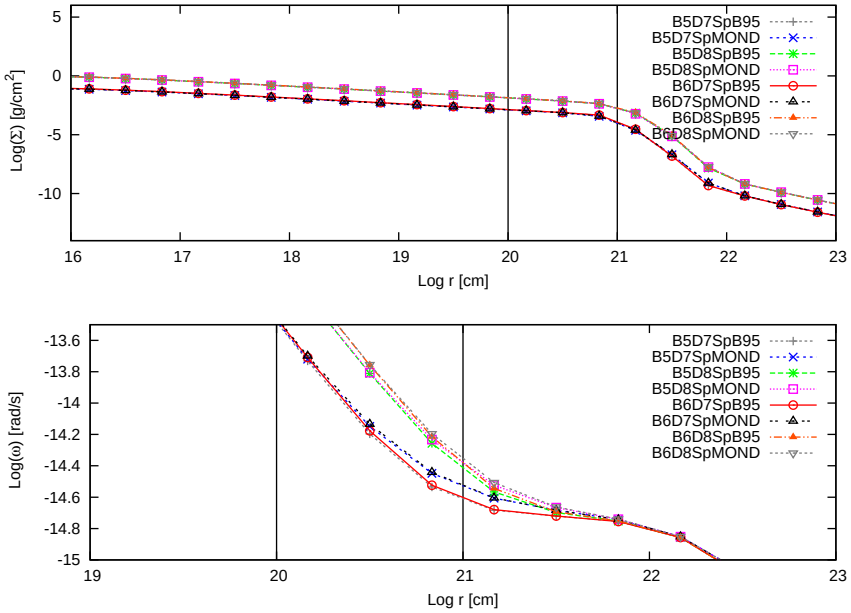

Figure 33: *Surface density and angular velocity (lower panel enlarged resolution) for low mass disk systems ($10^5 M_\odot$ and $10^6 M_\odot$ BH with $10^7 M_\odot$ and $10^8 M_\odot$ disks) embedded in a spiral galaxy potential. Using B95 dark matter halos and MOND gravity modification respectively. Careful examination of the angular velocity profile for the lowest mass systems reveals a difference in angular velocity at the edge of the disk systems before the angular velocity is dominated by the galactic potential. Additionally this plot demonstrates the importance of self-gravity. The degeneracy of the B5D7SpB95 and B6D7SpB95 models shows, that at larger radial distances the angular velocity is dominated by the disk mass for systems with a small central mass. This allows one to speculate, that the disk mass is also of importance for higher mass systems.*

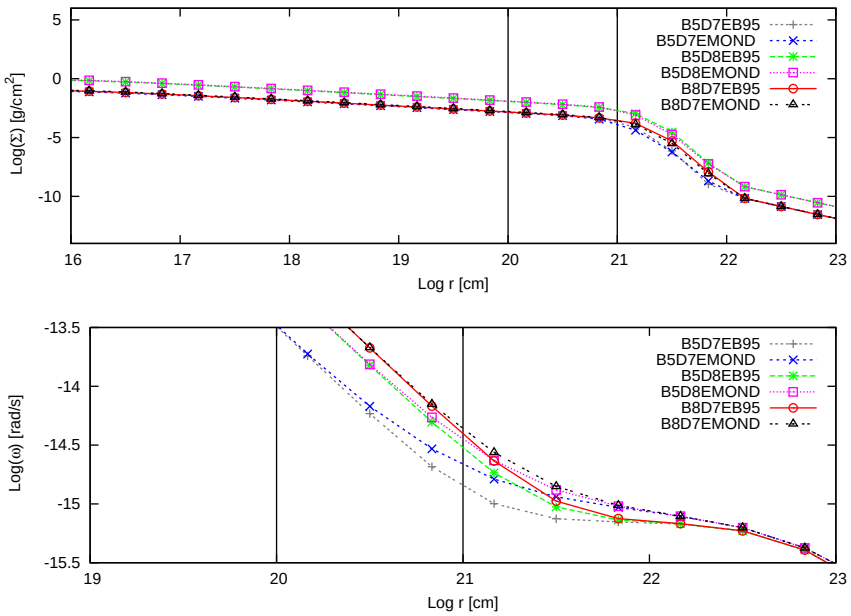

Figure 34: *Surface density and angular velocity (lower panel enlarged resolution) for low mass disk systems ($10^5 M_\odot$ and $10^8 M_\odot$ BH with $10^7 M_\odot$ and $10^8 M_\odot$ disks) embedded in an elliptical galaxy potential. Using B95 dark matter halos and MOND gravity modification, respectively. Careful examination of the angular velocity profile for the lowest mass systems reveals a difference in angular velocity at the edge of the disk systems, before the angular velocity is dominated by the galactic potential. Due to the smaller enclosed mass the system remains in the MOND regime over a larger radial extent and goes deeper into the MOND regime than the spiral system. The divergence in the galactically dominated radial extent is probably due to the smaller enclosed mass. In the relevant physical regime, however, the behavior is similar and can be explained by the same mechanism. Although these results show a larger deviation in an elliptical scenario, these are less likely to host the low mass systems that show the effect.*

Evolution-time

Fig.(27) shows that the embedding scenario chosen has a certain influence on the time a system needs to reach the quasi-stationary state. The profiles of the characteristic properties show that this state is also attained in the MOND scenarios, and is highly similar to that of the embedding in the galactic and B95 potentials. As described, the effective gravitational acceleration is larger in the MOND regime. This emulates the larger mass obtained by including a dark matter halo. However, for low mass systems there appear to be differences in e.g. the angular velocity. Thus it is possible that the evolution time-scales also display discrepancies. Fig.(35) shows the evolution time for a wide array of disk systems in the MOND and B95 scenarios in spiral potentials. The evolution of low mass systems is faster in the MOND scenario but, this is only the case for the extremely low mass systems. Apart from that the evolution displays the same characteristics of anti-hierarchical growth as previously described.
Fig.(36) shows that this is also the case for embedding in an elliptical host galaxy.

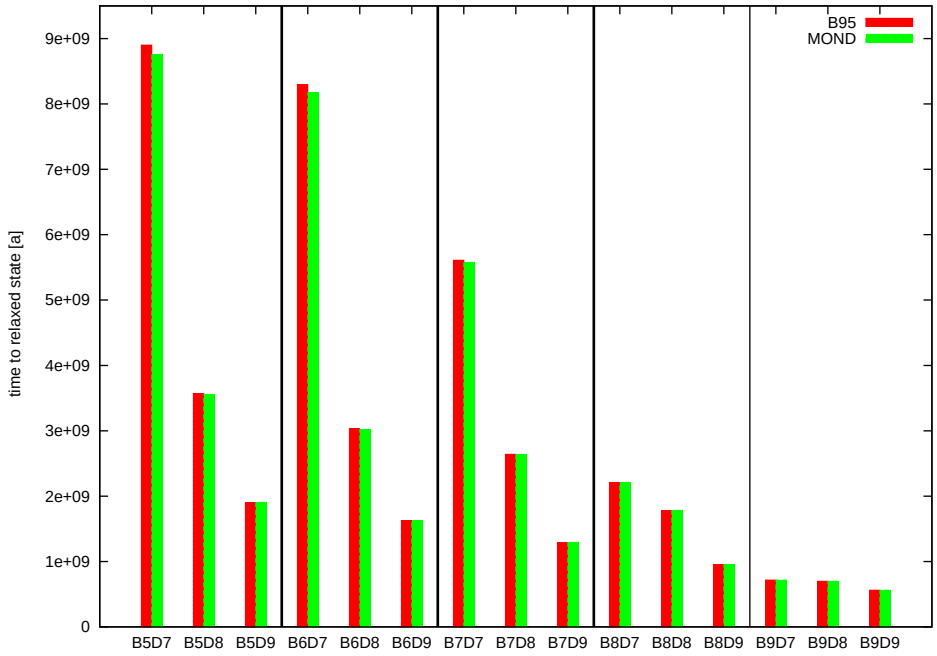

Figure 35: *Evolution time to the quasi-stationary state for various disk systems embedded in a spiral potential using a MOND scenario and a B95 dark matter profile. The evolution time of the very low mass MOND systems is marginally shorter than the B95 systems, due to the larger effective gravitational acceleration. The higher mass systems show no differences as they are not in the MOND regime. The trends of anti-hierarchical growth are clearly visible, with the greater importance of the central mass emerging clearly in the comparison of systems with the same total mass. In both scenarios larger disk masses also lead to shorter evolution time-scales*

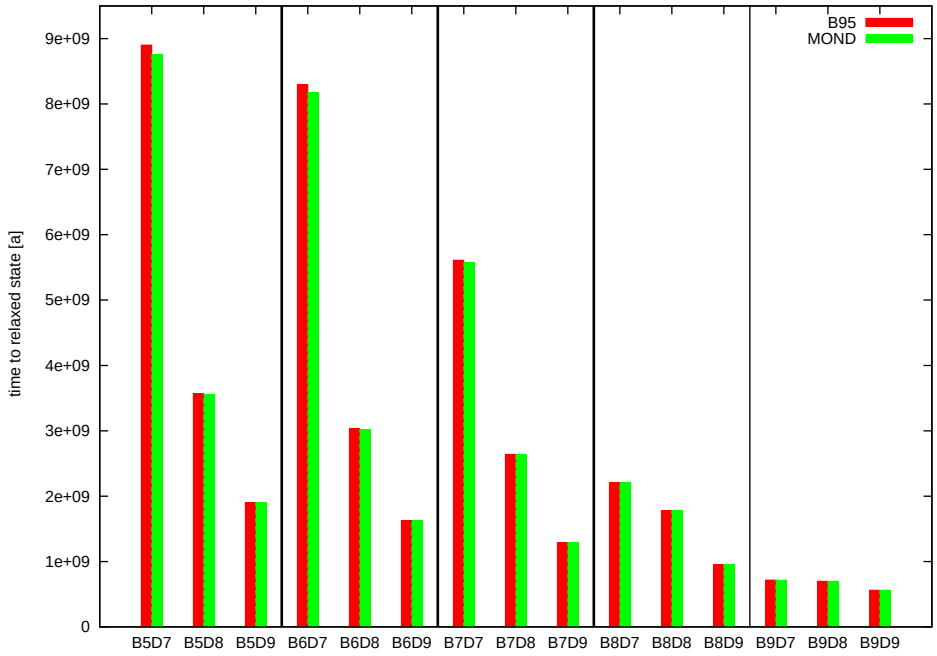

Figure 36: *Evolution time to quasi-stationary state for the same systems as in fig.(35) in B95 and MOND scenarios with an elliptical embedding scenario. The results are the same as for the case of spiral embedding.*

6.4 Constraints for Generalized Potentials

This work has used MOND as a proxy for acceleration scale based modifications to Newtonian gravity. The modification is characterized by a constant with the dimension of an acceleration a_0 and a function $\mu(x)$, which is only defined by its asymptotic behavior. For a given $\mu(x)$ the choice of the value of a_0 governs the location of the transition from Newtonian to MONDian gravity and thus, whether or not the system enters the MOND regime. The previous section has shown that it might be possible to use these systems to differentiate between different dark matter scenarios and modifications of gravity. This depends, however, on the value of the characteristic acceleration used. Fig.(37) and fig.(38) show that for a factor of 10 larger value of a_0 the difference would become far more significant, while a value for a_0 that is smaller by a factor of 10 would render accretion disks around super massive black holes useless as testbeds for these scenarios. Therefore, these systems can only be used to constrain the value of a characteristic acceleration upwards.
Additionally in the case of elliptical embedding it is unlikely to find such low mass systems in elliptical host galaxies.

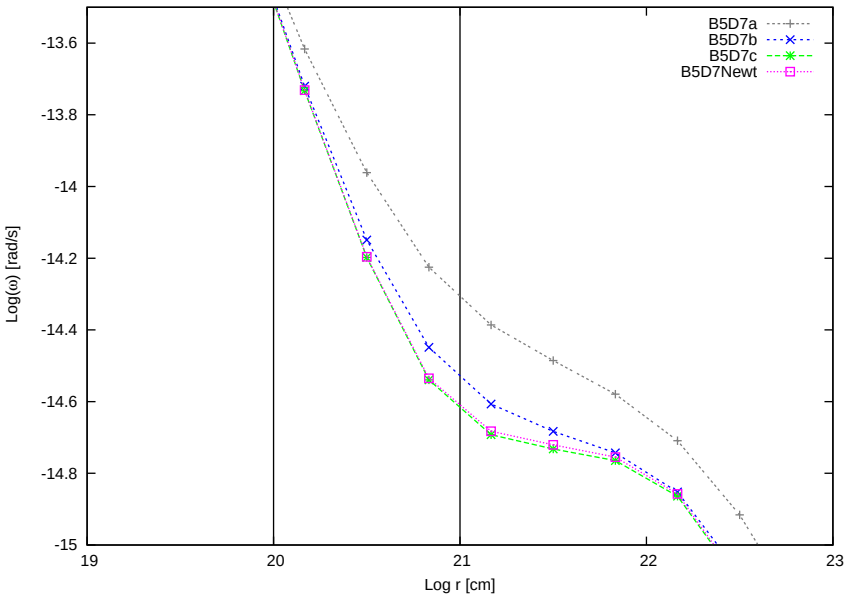

Figure 37: *Angular velocity for a* $10^5 M_\odot$ *BH with a* $10^7 M_\odot$ *disk embedded in a spiral galaxy. Three MOND scenarios with different values for* a_0 *are contrasted with a Newtonian B95 model. The MOND models are B5D7a(* $a_0 = 10^{-7}$ cms^{-2} *), B5D7b(* $a_0 = 10^{-8}$ cms^{-2} *) and B5D7c(* $a_0 = 10^{-9}$ cms^{-2} *). The larger value of* a_0 *leads to a much greater difference in angular velocity, as the system is further in the MOND regime. A much lower value for* a_0 *reinstates the degeneracy of the scenarios, as the system does not enter the MOND regime.*

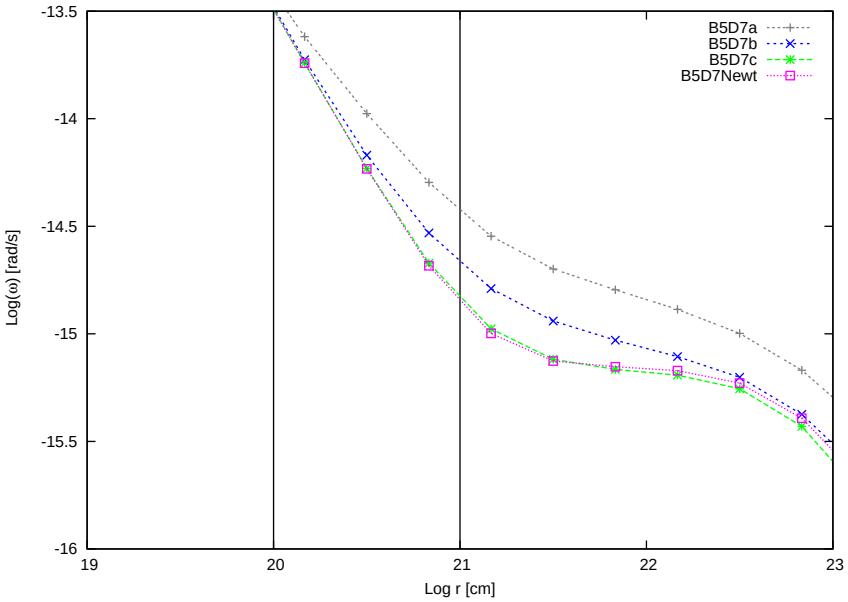

Figure 38: *Angular velocity for a* $10^5 M_\odot$ *BH with a* $10^7 M_\odot$ *disk embedded in an elliptical galaxy. Three MOND scenarios with different values for* a_0 *are contrasted with a Newtonian B95 model. The MOND models are B5D7a(* $a_0 = 10^{-7}$ cms^{-2} *), B5D7b(* $a_0 = 10^{-8}$ cms^{-2} *) and B5D7c(* $a_0 = 10^{-9}$ cms^{-2} *). The results agree with those obtained for spiral embedding. Such low mass systems in elliptical hosts are unlikely.*

7 Discussion and Outlook

The work presented here has used a simple model to test, whether embedding the accretion disks around super massive black holes in the background potentials, created by the matter distributions which surround them, has a discernable and relevant influence on their evolution. Additionally, the effect of of an acceleration-scale modification to Newtonian gravity has been investigated and the use of accretion disk systems around black holes as test-benches for differentiating between such modifications and the CDM paradigm has been tested. Due to the simplicity of the model used, this can be seen a s a feasibility / usefullness study for possible future work in this direction.

While the evolution of the inner regions of the accretion disk appears to be entirely dominated by the gravitational potentials of the central black hole and the mass distribution of the disk itself, the behavior of the disk at its edges is certainly influenced by the background potentials of the luminous host galaxy and the hosts dark matter halo. The disks appear constrained to smaller radii when embedded, with the surface density subsequently being somewhat higher. The radial outflow is then slowed somewhat, while the angular velocity increases. This in turn leads to a shorter viscous time-scale. As a whole the disk systems investigated evolve faster, the higher their total mass is, a result fitting the hypothesis of anti-hierarchical growth.

The evolution of the disk systems appears to be largely independent of the type of luminous host, as the relevant regions of the hosts density distribution display similar forms, i.e the disk lies in the bulge of a spiral galaxy which strongly resembles the inner regions of an elliptical galaxy. The scale relations for the embedding scenarios lead to an almost indistinguishable development, although this might be broken if dwarf galaxy types are taken into account. Additionally other potential perturbations that affect the central regions, such as bar instabilities might be of great interest for the development of these systems.

The angular velocity profiles of the disks may allow one to distinguish between cuspy halo profiles and constant density core profiles, and in the case of low mass systems, even enable a test of acceleration based modifications to gravity, if the acceleration scale is on the order of 10^{-8} cms^{-2} or larger. This could prove difficult however, as the surface densities at the disks edge for these low mass systems are fairly small, in addition to the edges being cold, leading to a small photon flux from these regions.

Given the fact that the disk has been assumed to be razor thin, the self-gravity of the disk has been treated using a monopole approximation, and the viscosity is parametrized, the results obtained here should be seen as an indication that there is a very real possibility that these scenarios will also show interesting physical effects if treated in more detail. Such a treatment could include, e.g. vertical structure for the disk and treatment of the disk not as a monopole but as an extended object.

Nevertheless the results show that embedding potentials, and possibly also generalized gravitational potentials in the form of modifications of gravity, influence the evolution of AGN type accretion disks and should be taken into consideration in the long run.

List of Figures

References

Abramowitz, M. & Stegun, I. A. (1972). *Handbook of Mathematical Functions*. Handbook of Mathematical Functions, New York: Dover, 1972

Bekenstein, J. & Milgrom, M. (1984, Nov.). Does the missing mass problem signal the breakdown of Newtonian gravity? *Astrophysical Journal 286*, 7–14

Bekenstein, J. D. (2004, Oct.). Relativistic gravitation theory for the modified Newtonian dynamics paradigm. *Physical Review D 70*(8), 083509–+

Binney, J. & Tremaine, S. (1987). *Galactic dynamics*. Princeton, NJ, Princeton University Press, 1987, 747 p.

Burkert, A. (1995, Jul.). The Structure of Dark Matter Halos in Dwarf Galaxies. *Astrophysical Journall 447*, L25+

Burkert, A. (2000, May). The Structure and Evolution of Weakly Self-interacting Cold Dark Matter Halos. *Astrophysical Journal, Letters 534*, L143–L146

Duschl, W. J., Strittmatter, P. A. & Biermann, P. L. (2000, May). A note on hydrodynamic viscosity and selfgravitation in accretion disks. *Astronomy and Astrophysics 357*, 1123–1132

Eckhardt, D. H. (1993, Oct.). Exponential potential versus dark matter. *Physical Review D 48*, 3762–3767

Eke, V. R., Navarro, J. F. & Steinmetz, M. (2001, Jun.). The Power Spectrum Dependence of Dark Matter Halo Concentrations. *Astrophysical Journal 554*, 114–125

Frank, J., King, A. & Raine, D. J. (2002, Feb.). *Accretion Power in Astrophysics: Third Edition*. Cambridge, UK: Cambridge University Press, February 2002, 384 p.

Fromang, S., Balbus, S. A., Terquem, C. & De Villiers, J.-P. (2004, Nov.). Evolution of Self-Gravitating Magnetized Disks. II. Interaction between Magnetohydrodynamic Turbulence and Gravitational Instabilities. *Astrophysical Journal 616*, 364–375

Hasinger, G., Miyaji, T. & Schmidt, M. (2005, Oct.). Luminosity-dependent evolution of soft X-ray selected AGN. New Chandra and XMM-Newton surveys. *Astronomy and Astrophysics 441*, 417–434

Hawley, J. F., Gammie, C. F. & Balbus, S. A. (1995, Feb.). Local Three-dimensional Magnetohydrodynamic Simulations of Accretion Disks. *Astrophysical Journal 440*, 742–+

Hayashi, E. & Matsuda, T. (2001, Mar.). Is Angular Momentum in an Accretion Disk Transported Inwards? *Progress of Theoretical Physics 105*, 531–536

Hernquist, L. (1990, Jun.). An analytical model for spherical galaxies and bulges. *Astrophysical Journal 356*, 359–364

Hinz, I. V. (2008). *Entwicklung Protostellarer und Protoplanetarer Akkretionsscheiben*. Diplomarbeit, Institut für Theoretische Physik und Astrophysik der Christian Albrechts Universität zu Kiel

Kuhn, J. R. & Kruglyak, L. (1987, Feb.). Non-Newtonian forces and the invisible mass problem. *Astrophysical Journal 313*, 1–12

Landau, L. D. & Lifschitz, E. M. (1959). *Course of Theoretical Physics Volume 6: Fluid Mechanics*. London, New York, Paris, Los Angeles, Pergamon Press Ltd., 1959, 536 p.

Lynden-Bell, D. & Pringle, J. E. (1974, Sep.). The evolution of viscous discs and the origin of the nebular variables. *Monthly Notices of the Royal Astronomical Society 168*, 603–637

Milgrom, M. (1983, Jul.). A modification of the Newtonian dynamics as a possible alternative to the hidden mass hypothesis. *Astrophysical Journal 270*, 365–370

Milgrom, M. (1986, Mar.). Solutions for the modified Newtonian dynamics field equation. *Astrophysical Journal 302*, 617–625

Miyamoto, M. & Nagai, R. (1975). Three-dimensional models for the distribution of mass in galaxies. *Publications of the Astronomical Society of the Pacific 27*, 533–543

Moore, B., Quinn, T., Governato, F., Stadel, J. & Lake, G. (1999, Dec.). Cold collapse and the core catastrophe. *Monthly Notices of the Royal Astronomical Society 310*, 1147–1152

Navarro, J. F., Frenk, C. S. & White, S. D. M. (1997, Dec.). A Universal Density Profile from Hierarchical Clustering. *Astrophysical Journal 490*, 493–+

Navarro, J. F., Hayashi, E., Power, C., Jenkins, A. R., Frenk, C. S., White, S. D. M., Springel, V., Stadel, J. & Quinn, T. R. (2004, Apr.). The inner structure of ΛCDM haloes - III. Universality and asymptotic slopes. *Monthly Notices of the Royal Astronomical Society 349*, 1039–1051

Paczynski, B. (1978). A model of selfgravitating accretion disk. *Acta Astronomica 28*, 91–109

Pringle, J. E. (1981). Accretion discs in astrophysics. *Annual Review of Astronomy and Astrophysics 19*, 137–162

Richard, D. & Zahn, J.-P. (1999, Jul.). Turbulence in differentially rotating flows. What can be learned from the Couette-Taylor experiment. *Astronomy and Astrophysics 347*, 734–738

Salucci, P. & Burkert, A. (2000, Jul.). Dark Matter Scaling Relations. *Astrophysical Journall 537*, L9–L12

Sanders, R. H. (1984, Jul.). Anti-gravity and galaxy rotation curves. *Astronomy and Astrophysics 136*, L21–L23

Sanders, R. H. (1986, Dec.). Alternatives to dark matter. *Monthly Notices of the Royal Astronomical Society 223*, 539–555

Sanders, R. H. & McGaugh, S. S. (2002). Modified Newtonian Dynamics as an Alternative to Dark Matter. *Annual Review of Astronomy and Astrophysics 40*, 263–317

Satoh, C. (1980). Dynamical Models of Axisymmetric Galaxies and Their Applications to the Elliptical Galaxy NGC4697. *Publications of the Astronomical Society of the Pacific 32*, 41–+

Shakura, N. I. & Syunyaev, R. A. (1973). Black holes in binary systems. Observational appearance. *Astronomy and Astrophysics 24*, 337–355

Thompson, R. I., Strittmatter, P. A., Erickson, E. F., Witteborn, F. C. & Strecker, D. W. (1977, Nov.). Observation of preplanetary disks around MWC 349 and LKH-alpha 101. *Astrophysical Journal 218*, 170–180

Tohline, J. E. (1983). Stabilizing a cold disk with a 1/r force law. In *Internal Kinematics and Dynamics of Galaxies*, ed. E. Athanassoula, Volume 100 of *IAU Symposium*, 205–+

Ueda, Y., Akiyama, M., Ohta, K. & Miyaji, T. (2003, Dec.). Cosmological Evolution of the Hard X-Ray Active Galactic Nucleus Luminosity Function and the Origin of the Hard X-Ray Background. *Astrophysical Journal 598*, 886–908

Zhao, H. S. & Famaey, B. (2006, Feb.). Refining the MOND Interpolating Function and TeVeS Lagrangian. *Astrophysical Journal, Letters 638*, L9–L12

Acknowledgements

First of all, I would like to thank my supervisor Prof. Dr. Wolfgang J. Duschl, for being extremely flexible and allowing me to combine many interesting questions into the project presented here. I enjoyed working on the subject, and the way I was allowed to work on it independently, but with the knowledge that I could consult him if necessary, has motivated and enabled me to decide to continue working in this field.

I would like to thank J.Navarro, for kindly allowing me to use his code and giving me some pointers on its use.

Danksagung

Ich möchte mich bei der ganzen Arbeitsgruppe bedanken für die tolle Atmosphäre und die schönen gemeinsamen Erlebnisse. Besonderer Dank an dieser Stelle an Daniel Asmus (und nochmal extra für das Durcharbeiten meiner Arbeit) und Marc Junker, meine Bürogenossen, sowie an Alexandra Tachil, Björn Sperling und Jan Hofmann.
Ebenfalls möchte ich mich bei B. Kuhr und H. Boll bedanken, ohne deren Mühen hier nichts laufen würde.

Dann möchte ich mich noch bei Nina Dresing, Thomas Möller und all die anderen netten Menschen, die ich während des Studiums kennegelernt habe, für die tolle Zeit bedanken.

Ein ganz grosses Dankeschön auch an meine WG. Daniel Viain, Johannes Köhler-Kaess, Leon Schramm und Tobias Bieler. Mit euch zusammen zu wohnen hat soviel Spass gemacht! Immer wenn mir die Uni mal zu viel wurde, habt ihr das Ganze in Perspektive gerückt. Vielen Dank!! Ihr wisst was ihr mir bedeutet. Danke auch an all die anderen, wundervollen Menschen in meinem Leben, ich habe einfach zu wenig Platz hier.

Schliesslich möchte ich mich noch bei meinen Eltern Pieter und Grada bedanken.
Bedankt vor al de raad en ondersteuning die jullie mij in de loop der tijd hebben gegeven. Jullie hebben mij nooit onder druk gezet en mij juist daardoor angedreven het meeste uit mijn mogelijkheden te maken. Bedankt vor alles jongens!

En nog één laatste person zou ik graag opnoemen. Mevr. Marie Grootes-Leeuw. Dit is ook voor u Oma!

Eidesstattliche Erklärung

Hiermit erkläre ich, die vorliegende Arbeit selbstständig und unter ausschliesslicher Verwendung der angegebenen Literatur und Hilfsmittel erstellt zu haben.

Kiel, den ——————————— ———————————

Meiert Willem Grootes